AD-A131 601 EXPERIMENTAL STUDY OF DISSOCIATIVE ATTACHMENT IN OPTICALLY-PUMPED LITHIUM..(U) AVCO EVERETT RESEARCH LAB INC EVERETT MA M W MCGEOCH ET AL. MAY 83 1/1

UNCLASSIFIED AFOSR-TR-83-0725 F49620-82-C-0051 F/G 20/8 NL

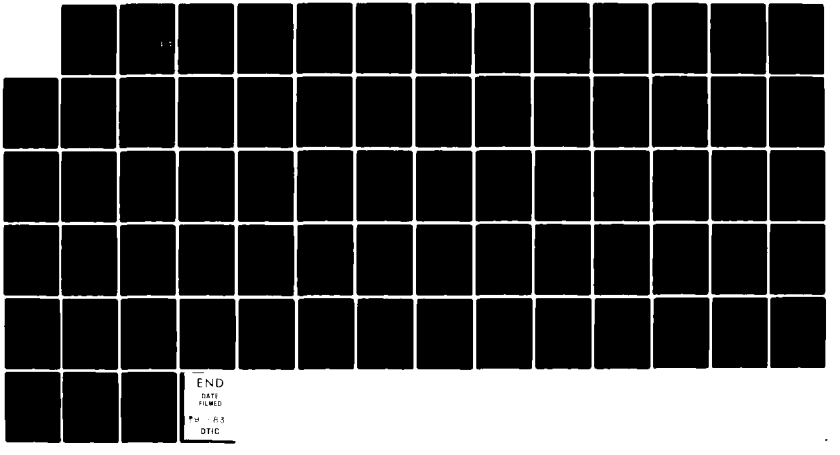

END

DATE FILMED

8-83

DTIC

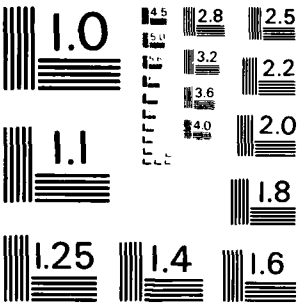

EXPERIMENTAL STUDY OF DISSOCIATIVE ATTACHMENT IN OPTICALLY–PUMPED LITHIUM MOLECULES

Malcolm W. McGeoch and Robert E. Schlier
AVCO EVERETT RESEARCH LABORATORY, INC.
a Subsidiary of Avco Corporation
2385 Revere Beach Parkway
Everett, Massachusetts 02149

May 1983
Final Report for Period 1 May 1982 – 30 April 1983

Prepared for

AIR FORCE OFFICE OF SCIENTIFIC RESEARCH
Washington, D.C.

UNCLASSIFIED

SECURITY CLASSIFICATION OF THIS PAGE (When Data Entered)

REPORT DOCUMENTATION PAGE	READ INSTRUCTIONS BEFORE COMPLETING FORM
1 REPORT NUMBER: AFOSR-TR- 83-0725	2. GOVT ACCESSION NO.: AD-A131 601
	3. RECIPIENT'S CATALOG NUMBER
4 TITLE (and Subtitle): EXPERIMENTAL STUDY OF DISSOCIATIVE ATTACHMENT IN OPTICALLY-PUMPED LITHIUM MOLECULES	5. TYPE OF REPORT & PERIOD COVERED: Final Report 5/1/82 - 4/30/83
	6 PERFORMING ORG. REPORT NUMBER
7. AUTHOR(s): Malcolm W. McGeoch, Robert E. Schlier	8. CONTRACT OR GRANT NUMBER(s): F49620-82-C-0051
9 PERFORMING ORGANIZATION NAME AND ADDRESS: Avco Everett Research Laboratory, Inc. 2385 Revere Beach Parkway Everett, MA 02149	10 PROGRAM ELEMENT, PROJECT, TASK AREA & WORK UNIT NUMBERS: 61102F 2301/A7
11 CONTROLLING OFFICE NAME AND ADDRESS: Air Force Office of Scientific Research Washington, DC	12 REPORT DATE: 5/83
	13. NUMBER OF PAGES: 73
14 MONITORING AGENCY NAME & ADDRESS(if different from Controlling Office)	15. SECURITY CLASS. (of this report): Unclassified
	15a DECLASSIFICATION DOWNGRADING SCHEDULE

16 DISTRIBUTION STATEMENT (of this Report)

Distribution Unlimited

Approved for public release; distribution unlimited.

17 DISTRIBUTION STATEMENT (of the abstract entered in Block 20, if different from Report)

18 SUPPLEMENTARY NOTES

19 KEY WORDS (Continue on reverse side if necessary and identify by block number)

Lithium
Dissociative Attachment
Optical Pumping (of lithium molecules)
Lithium Supersonic Beam
Lithium Rotational Temperature

20 ABSTRACT (Continue on reverse side if necessary and identify by block number)

Details are presented of an experimental study which has as its goal the observation of lithium negative ions by the process of dissociative attachment in optically-pumped lithium dimer molecules. A description is given of a new lithium supersonic beam apparatus with a slit nozzle and gravitational recirculation of the molten lithium. The source operates up to 900°C and yields a lithium density of 1 x 10^{14} cm^{-3} at 10 cm downstream from the slit. The

DD FORM 1 JAN 71 1473 EDITION OF 1 NOV 65 IS OBSOLETE

UNCLASSIFIED

SECURITY CLASSIFICATION OF THIS PAGE (When Data Entered)

beam density is modelled as a function of spatial coordinates. Two- and three-step photoionization of lithium dimers and lithium atoms has been performed using multiple, tunable nitrogen-pumped dye lasers. An electron density of up to 10^{10} cm^{-3} has been created in the beam. Using the lithium dimer ion signal the beam rotational temperature has been measured to be 150°K. Optically pumping experiments have been performed to create densities of up to 1×10^{11} cm^{-3} lithium molecules in vibrational states with $\nu = 10$. A preliminary search for negative ions has been made, which has determined an upper bound of 2×10^{-8} cm^3 sec^{-1} for the dissociative attachment rate constant for lithium dimer molecules in the states around $\nu = 10$.

TABLE OF CONTENTS

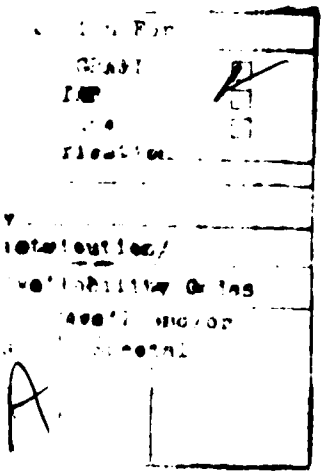

LIST OF ILLUSTRATIONS

1.0 INTRODUCTION

1.1 EXPERIMENTAL AIMS

The aim of this experimental program is to demonstrate, if possible, a new volume source of Li^- ions. The motives for this are three-fold:

1. Such a source would have the potential for being very 'cold' and hence would be ideal for the generation of highly directional neutral beams in space.[1]
2. A source of Li^- ions would be of interest in the Mirror Fusion program[2] as leading to more efficient reactor configurations.
3. There is intrinsic interest in new methods for the volume production of negative ions in general. The work with Li would be an excellent paradigm for the other alkali metals. Being a molecule of relatively few electrons there could be a benefit from this experiment to the development of theoretical models of dissociative attachment.

Based on the anticipated curve crossing of the repulsive $Li_2^- \, ^2\Sigma_g^+$ state with the bound $Li_2 \, X \, ^1\Sigma_g^+$ state (Figure 1) a high rate of dissociative attachment is expected for vibrationally excited Li_2 molecules, by the following process

$$Li_2 \, X \, (v^*) + e^- \rightarrow Li + Li^- \qquad (1\text{-}1)$$

With reference to Figure 1 it may be seen that the threshold vibrational level for zero energy dissociative attachment is somewhere above $v = 16$. Its precise location depends upon the as yet unmeasured portion of the $Li_2^- \, ^2\Sigma_g^+$

1. 'Proposal for Experimental Study of Dissociative Attachment in Optically Pumped Lithium Molecules,' AERLP 553, September 1981.
2. 'Light Atom Neutral Beams for Tandem Mirror End Plugs,' Post, D.E., Grisham, L.R., Santarius, J.F., and Emmert, G.A., Nucl. Fusion, 23, 3 (1983).

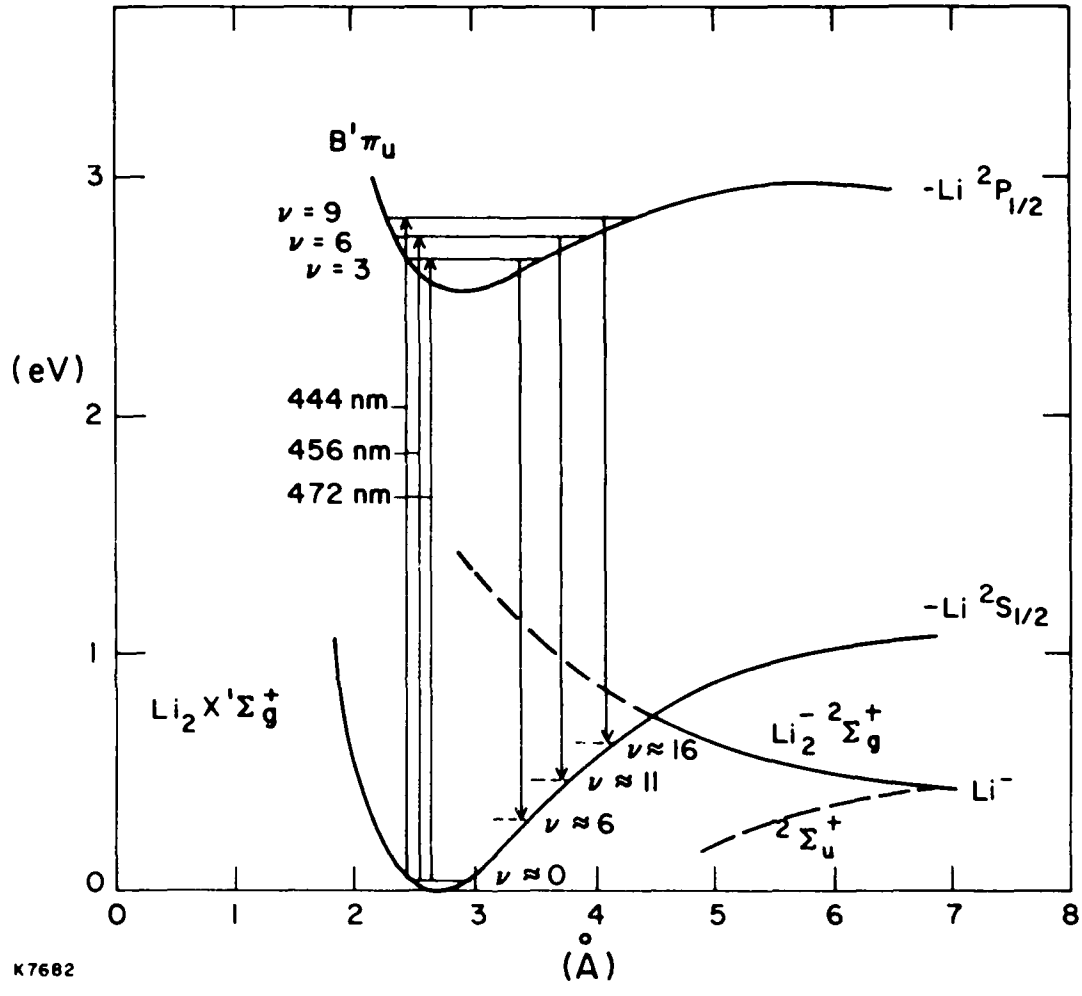

Figure 1 Illustration of Li_2 Vibrational Pumping

repulsive potential. If attachment occurs at threshold, the Li and Li^- products share equally a total kinetic energy of ≈ 0.3 eV, so that very cold (0.15 eV) Li^- are produced.

It was proposed by AERL[1] to create a population of metastable Li_2 X (v^*) states in an optically-pumped supersonic Li beam, and to introduce electrons by multiple-step photoionization of Li in the beam. A supersonic beam is necessary for several reasons:

1. Li_2 (v^*) is completely metastable in the collision-free part of the beam, and hence a large v^* population may be maintained for a reaction time of many tens of microseconds.
2. The beam density is low ($\approx 1 \times 10^{14}$ cm^{-3}) and the beam has only a few centimeters of lateral extent, so that Li^- ions may be extracted laterally into vacuum without excessive collisional destruction.
3. The vibrational manifold of Li_2 molecules in the beam is relaxed almost completely to the $v = 0$ state, and the rotational temperature is relaxed to the 30°K to 150°K range, giving a compact band structure of optical excitation of Li_2 via the X - B absorption.

The method proposed for optical excitation is to pump the Li_2 (X - B) band and take advantage of the favorable Frank-Condon factors for radiative B → X decay, which leave ≈ 50 percent of pumped molecules in a close group of vibrational states in the X manifold. Figure 1 illustrates this process for three different pump wavelengths.

An experiment which creates these conditions has been constructed and operated in the first year of work on this program at AERL. The current state of progress is reviewed in the following subsection, which overviews the more detailed discussions of Section 2 and Section 3.

1.2 OVERVIEW OF EXPERIMENTAL PROGRESS TO DATE

To date we have placed on experimental upper bound on the dissociative attachment rate constant from $v = 11$ of $k_{DA} \lesssim 2.4 \times 10^{-8}$ cm^3/sec^{-1} (Section 3.7), a number which reflects the rather poor resolution of our initial experiments. In these experiments we have employed two different lasers for optical pumping:

1. A N_2-pumped dye laser, which only accessed ≈ 8 percent of the Li_2 population (Section 3.5).
2. A flashlamp-pumped dye laser, which pumped up to 40 percent of the Li_2 molecules, but had operating defects which greatly hampered the collection of data (Section 3.6).

In spite of its deficiencies the broad-band pumping with the flashlamp dye laser permitted the best experimental resolution and is the route proposed to reach a sensitivity down to 10^{-13} cm^3/sec^{-1} in future experiments (Section 4.0).

After some initial difficulties the recirculating Li beam apparatus worked well, and according to general expectation. To our knowledge this is the first slit nozzle Li source with recirculation to be built. Its uses for Li_2 spectroscopy are many and one of the most significant is proposed in Section 4.2: measurement of the photoionization spectrum of the Li_2 (B) state.

The density and temperature of the supersonic beam in the experimental region (10 cm from the slit nozzle) have been characterized in some detail (Section 3.1). This procedure was necessary in order to gain a quantitative estimate of the Li_2 (v^*) density, and hence of k_{DA}. The rotational temperature was estimated by comparison of the Li_2^+ spectrum with computed band spectra (Section 3.4). This represents the first available temperature information on a slit nozzle beam of alkali dimers. It also represents the first observations of a Li_2^+ spectrum via tunable two-step photoionization. (Previously the two-step process had been observed in a hot effusive beam with Ar^+ ion laser excitation.)

The limited resolution obtained to date is due to:

1. Operation of the Li oven at 800°C rather than its maximum of 920°C because of a fault in the heating system which requires stripping down for repair. To strip, re-assemble, bake, re-charge with Li and bring the oven to temperature takes up to 2 weeks. As a result of the reduced temperature the Li_2 (v^*) density was lower by 8 times than the maximum obtained.
2. Unsatisfactory performance of the existing flashlamp-pumped dye laser, as discussed in Section 3.6, which led to a 10 times increase in background noise.

3. The use of small laser beam radii (0.1 cm) which gave a reduced e^-, Li_2 interaction time due to rapid expansion of the plasma column (Section 3.3). With 0.5 cm beam radius a five times longer interaction period is available.

The net effect of the above three items together was to reduce the experimental resolution by more than a factor of 10^2. Further experimentation using a new laser will enable $k_{DA} < 10^{-10}$ cm^3/sec^{-1} to be resolved using Li^+ photoionization (Section 4.1).

In conclusion, although we consider that good exp[illegible]mental progress has been made to date, there is scope for further work in [illegible]ch considerably improved results should be obtained.

With respect to Li^- source performance, a k_{DA} val[illegible] of 10^{-8} cm^3/sec^{-1} would be good, whereas 10^{-9} cm^{-3}/sec^{-1} would be on the [illegible] side. In theory there should be high enough rates from the vibrational levels close to the curve crossing point. The experimental aim is to seek the appropriate levels.

1.3 SUMMARY OF FUTURE EXPERIMENTS

As detailed in Section 4.1 there is considerable scope for increased sensitivity in the present measurements of dissociative attachment. A continuation of the present program is proposed in which higher Li_2 and electron densities are to be used in a geometry which allows a longer time for interaction. The resolution level is calculated to be 1×10^{-13} cm^3/sec^{-1}.

It is proposed (Section 4.2) to take advantage of the present experimental capability to perform a new and fundamental measurement of molecular photoionization, from the Li_2 (B) state.

If dissociative attachment is observed in the proposed experiments, measurements will be made of its vibrational state and electron temperature dependence, with a view to providing a framework for the design of future Li^- sources.

2.0 EXPERIMENTAL APPARATUS

2.1 DESIGN OF A RECIRCULATING LITHIUM VAPOR SOURCE

The vapor pressure of lithium required to provide a reasonably dense supersonic lithium beam that contains a reasonably large fraction of lithium dimers is on the order of 10 torr. At this pressure and with a slit source area of about 0.1 cm^2, the mass flow through the slot is on the order of 100 g/hr. In order to provide reasonable experimentation times, one must either use inordinately large amounts of lithium, or employ some form of recirculation.

We have chosen the latter course, since it avoids the necessity of handling large quantities of lithium, which is a hazardous material. Recirculation systems can be constructed utilizing pumps to force the liquid metal back into the source oven, or utilizing gravitational forces to retrun the liquid to the oven. The latter approach is less complex and requires a much smaller apparatus. This fits well with the vacuum system and laser sources that are available for the lithium negative ion source experiments.

The vapor source must be heated to temperatures of up to 1000°C during operation. In order to obtain a sufficiently high vapor pressure, electron bombardment rather than resistance heating was chosen as the heating method, since the necessary power supplies were already available, and we have had considerable experience with electron bombardment heating of a uranium vapor source.

The vapor source is shown in Figure 2. The electron bombardment is provided by 10 filaments, operated in parallel, with the filaments being maintained at a negative potential and the source grounded. The electron emission from each pair of filaments is separately controlled, so that the source temperature can be balanced properly. The source is 24 in. long, and the filaments are separated by a distance of 0.25 in., with the upper filaments being 1.5 in. below the top of the source crucible. The filament pairs are located opposite to each other.

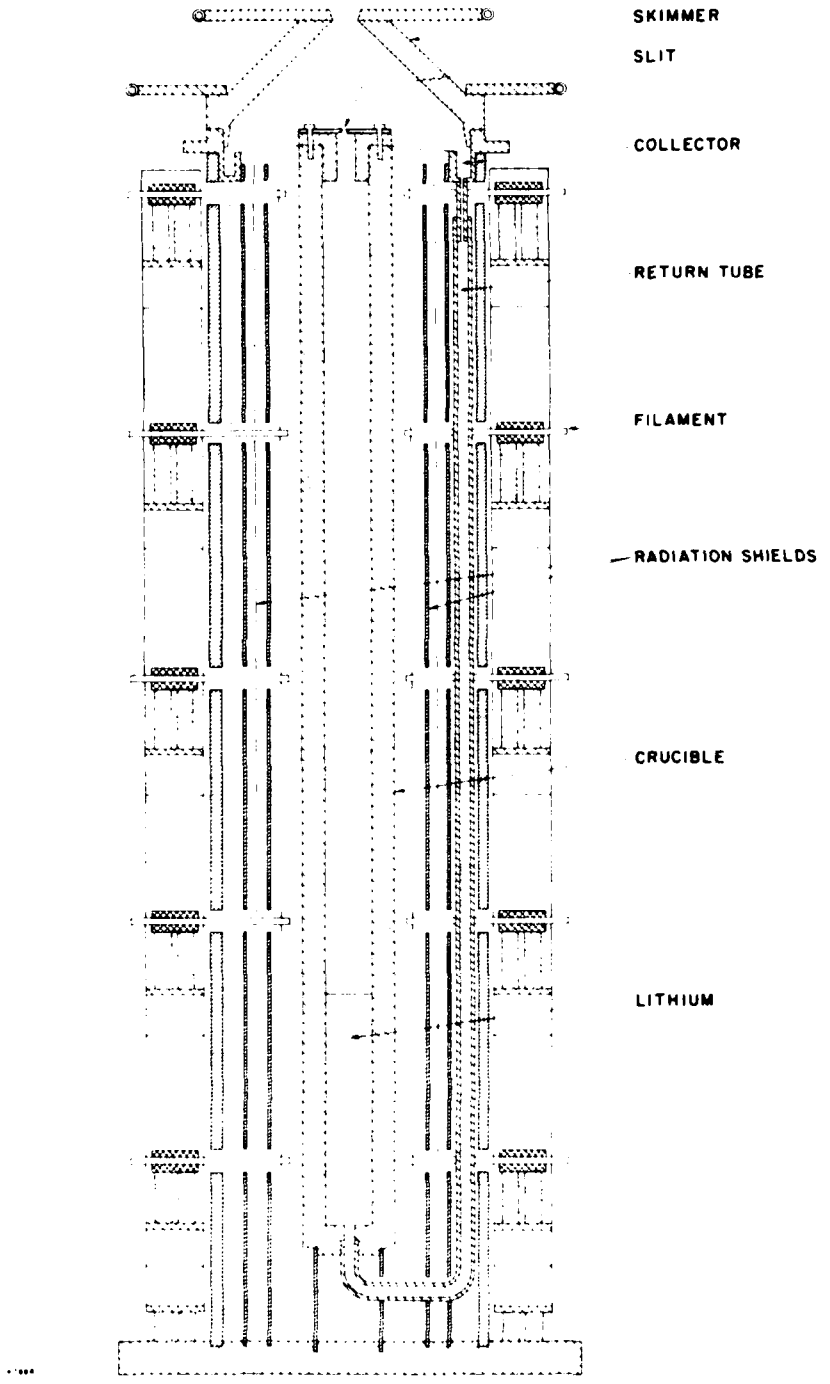

Figure 2 Scale Drawing of the Recirculating Li Beam Source (Crucible is 24 in. long)

The crucible was machined from a 2 in. diameter bar of 304 stainless steel, with a 1 in. diameter hole gun-drilled to 1 in. from the bottom. The return tube was heliarc welded to the bottom of the crucible. The heat shields were constructed from 304 stainless steel pipe. The original design had three heat shields, of 3.5, 4.5, and 6 in. outer diameter, with thicknesses of 0.065, 0.065, and 0.25 in., respectively. Two additional thin walled (0.025 in.) shields were inserted in order to reduce the overall power requirements. We estimated that about 2000 W would be required to heat the crucible to a minimum temperature of 900°C. This is well within the capability of the filament and power supply, which can deliver 500 mA at 6000 V.

Figure 3 shows the details of the source slit, skimmer, and lithium collection system. The slit is made up of two stainless steel half-circles which are bolted to the top of the cap which is attached to the top of the crucible. A slit opening of 0.025 in. has been used. A thin (0.025 in.) sheet of stainless steel is welded to the inner edge of the collector, and is held between the top of the crucible and the cap. In the original design, the edge of the sheet merely overlapped the collector, and sufficient lithium penetrated into the interior of the heat-shielded region to cause an electrical discharge. In operation, lithium which leaves the source and does not pass through the opening in the skimmer flows down the interior of the cone and collects in the well of the collector. It then flows through a 3/16 in. diameter tube into the 3/8 in. diameter return tube.

The system is charged with ~ 4 cu. in. of lithium metal, which when melted fills the bottom of the crucible to a depth of about 5 in., leaving a length of 15 in. between the top of the liquid level and the top of the crucible. Thus we can operate the source at internal pressures corresponding to 18 in. of lithium or a vapor pressure of about 18 torr, which requires that the lowest temperature of any part of the crucible not exceed about 920°C. We estimate, from a thermal analysis of the crucible, that the temperature midway between the filaments will be, at most, 80°C lower than the temperature near the filaments. The measurement thermocouples are located at the level of the filaments, so that if the temperature of the melt (the lowest thermocouple location) is 920°C, the temperatures at the other thermocouple location must be maintained 80 degrees higher. In practice, the temperature difference will be

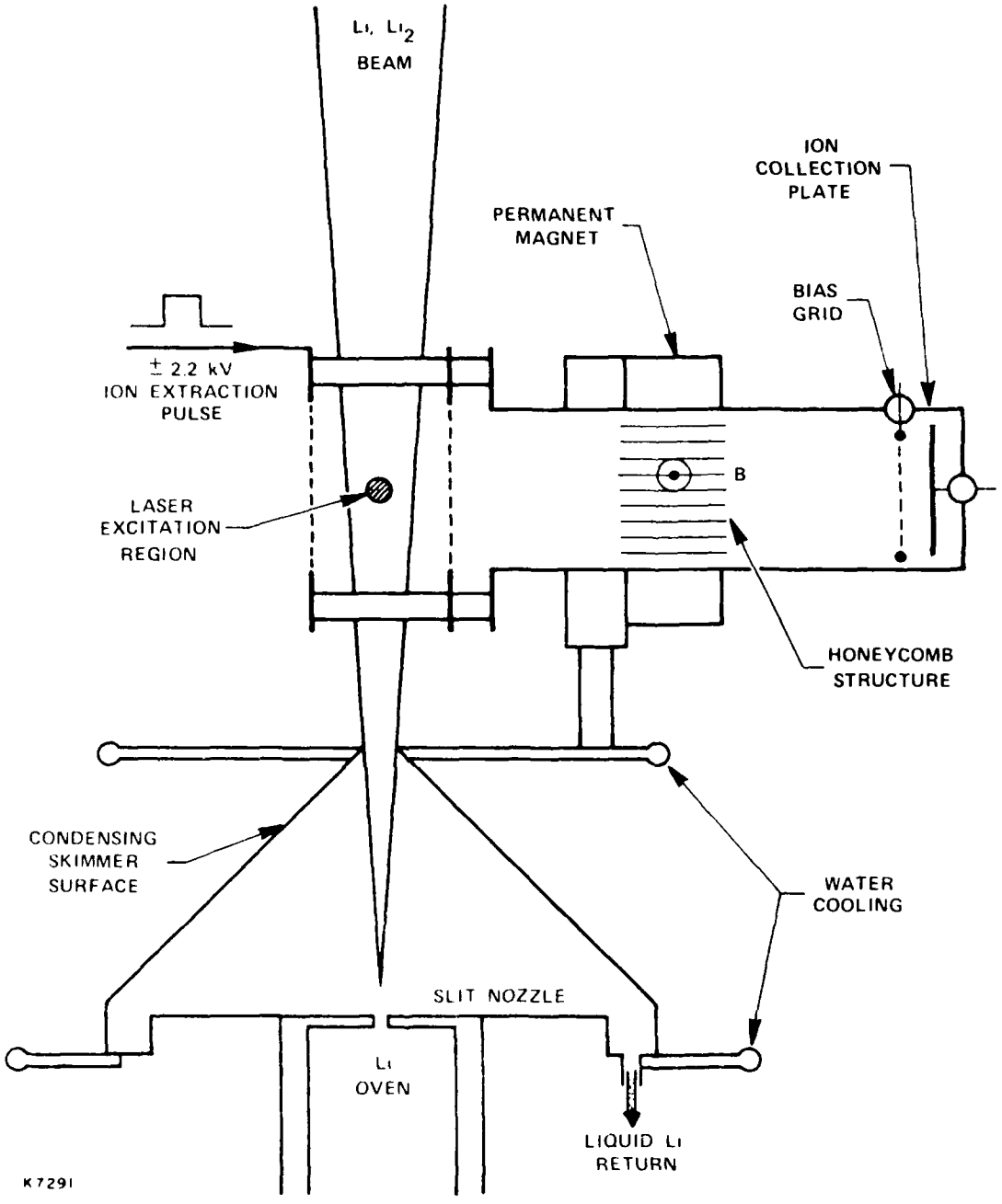

Figure 3 Schematic of Source Slit, Skimmer, Extraction Plates and Ion Drift Tube

less than this because of internal radiation conduction and lithium vapor conduction. We have observed, in early experiments with the empty crucible, that the temperature of the nozzle is about 50 degrees lower than the temperature at the uppermost filament.

In order for the recirculation of lithium to occur, it is necessary that the temperature of the skimmer and collector be above the melting point of lithium (186°C). On the other hand, if the temperature is too high, the density of the lithium re-evaporated from the inside of the skimmer and the collector will interfere with the flow of the beam from the slit source. This maximum temperature is estimated to be abut 400°C. Water-cooled rings are attached to the skimmer and collector to keep the temperature from exceeding the limit.

2.2 OPERATION OF THE LITHIUM SOURCE

The lithium source has a very large thermal mass, in part because it was necessary to have a thick-walled crucible, and also to ensure that heating power fluctuations did not affect the mean temperature appreciably. As a result, two to three hours are required to bring the crucible up to operating temperature. If the crucible is heated too rapidly, the temperature of the skimmer, collector, and return tubing will not reach the lithium melting point before appreciable vaporization has occurred, and lithium will collect in the upper part of the system.

The temperature at the skimmer is also critical since it must be above the melting point, but below that at which re-evaporation can become important. If there is excessive evaporation the density in the region between the source and the skimmer will become large enough so that interference with the flow can result. The skimmer and edge of the collector are attached to water-cooled plates to maintain a sufficiently low temperature.

In one case, the oven was heated at a total power of 1600 W and the liquid temperature reached an equilibrium value of 776°C. Under these conditions the temperature at the upper filament was 870°C and the skimmer and collector temperature ranged frm 272°C at the skimmer opening to 345°C at the collector. Under these conditions the total re-evaporation from the skimmer and collector

was estimated to be abut 0.1 g/hr, whereas the flow through the slot was about 8 g/hr. This amount of re-evaporation is insufficient to adversely affect the Li beam. At the highest temperature of the liquid (920°C) we would expect that the skimmer and collector temperatures would range from 325°C to 410°C, with a re-evaporation rate of 1.15 g/hr, compared to a flow of about 70 g/hr through the slot. The estimation of mass flow is discussed in Section 3.1 where a worst-case calculation of the skimmer evaporation rate is shown in Figure 6, being based upon a uniform highest-temperature assumption.

2.3 EXCITATION LASERS

A schematic of the experimental arrangement is shown in Figure 4. Three of the lasers are nitrogen laser-pumped dye cell oscillator amplifier combinations, and the fourth laser is a flashlamp-pumped dye cell oscillator.

The N_2-pumped lasers are grating tuned with a bandwidth of about 0.25 Å and an output of about 10 μJ in a 5 nsec pulse. Two of these lasers are used to excite and photo-ionize the lithium atoms in the extraction region and the third is used to excite (and photoionize) a portion of a selected lithium dimer band.

The output of the three N_2-pumped lasers can be combined with beam splitters and focussed on a removable external aperture which is in turn imaged on the extractor region. By this means the overlap of beams and the size of the beam can be controlled.

For ionization of the Li atoms, lasers at 671 nm and 611 nm were pulsed simultaneously. The third N_2-pumped dye laser was tuned in the range from 4500 Å to 4800 Å to excite a portion of the various ground state lithium dimer rotational bands. This laser was pulsed about 0.5 μsec prior to the other two lasers.

The flashlamp-pumped laser was tuned by the insertion of two pellicles (4 μm and 8 μm thick, respectively) in the laser cavity and adjusting their angle. With the 8 μm pellicle alone two possible wavelengths could be selected in the fluorescence band of the laser dye (Coumarin 450 or 460) and the second pellicle allowed selection of the desired wavelength. This laser had an output of about 2 mJ/pulse and a duration of about 1 μsec. It was fired about

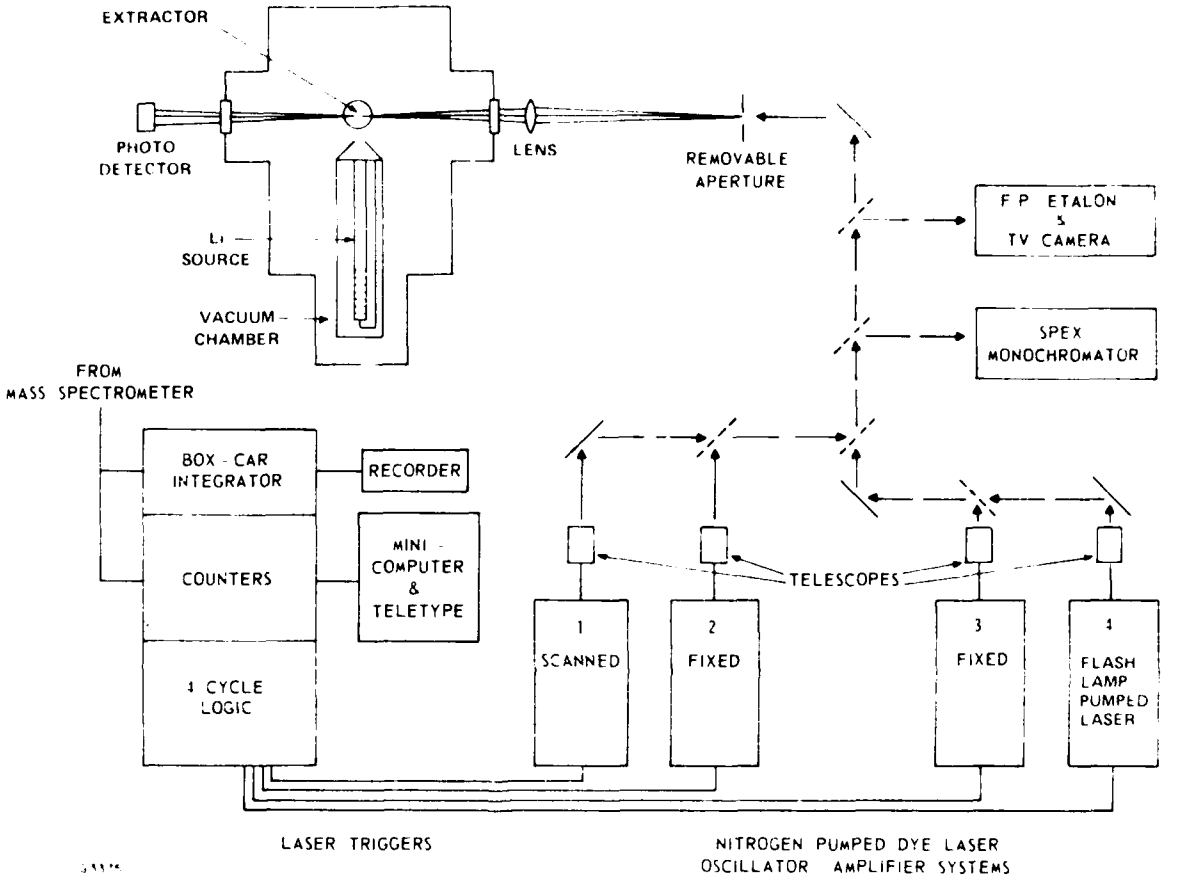

Figure 4 Schematic of the Experimental Arrangement

1.5 μsec prior to the Li photoionization lasers. The bandwidth was measured to be about 8 Å.

2.4 ION COLLECTION

Li^+, Li_2^+ or Li^- ions are extracted from the Li beam by the application of a pulsed electric field. The extraction voltage pulse is applied to two plane parallel mesh electrodes as shown in Figure 3. Ions travel down a 5 cm diameter, 20 cm long flight tube and are collected on a plate which inputs to an electrometer amplifier. The plate is at ground potential, but a battery-supplied bias grid 1 cm in front of it can be used to control secondary emission from the plate, or low energy charged particles in the flight tube.

Approximately at the mid-point of the flight tube there is a region of magnetic field perpendicular to the axis of the tube. This 200 G crossed field causes extracted electrons to bend in a radius of $\approx$ 1 cm and strike the walls of a honeycomb insert in the field. The field is high for only 4 cm of the drift path and ions are deflected by relatively small angles. It is calculated in Section 3.2 that for an extraction voltage of 2.2 kV (i.e., an ion energy of 1.1 kV) that only $\approx$ 25 percent of ions miss the collector plate due to magnetic deflection. When the polarity of the extraction voltage is reversed the electron signal is less than the system noise level, which represents $< 1 \times 10^{-4}$ of the positive ion signal. Because we may assume that negative ions are collected with the same efficiency as positive ions, the resolution of the experiment is such that we may detect the attachment of 1 in 10^4 electrons. The chamber pressure of $\approx 1 \times 10^{-6}$ torr is sufficiently low for collisional losses of negative ions in the flight tube to be negligible.

The Li^+ signal obeys the expected time dependence of a group of particles at 1.1 keV. Generally we have operated the signal detector at too high an impedance to resolve the time-dependence of a negative ion signal, but its presence cannot be confused with the electron signal because of the very complete suppression of the latter in the crossed field.

A 'boxcar' integrator is used to average the 60 Hz data signal over periods of up to 30 sec. Line interference which is present on the signal due to the Li oven heater currents is subtracted out by a separate sampler immediately before the photoionization pulse. It was found initially that the 1 μsec, 2.2 kV extractor pulse was coupling into the high impedance amplifier. This problem was almost completely eliminated by thorough electrical screening of the leads within the chamber and decoupling of the extractor electrodes from the flight tube body by ceramic standoff insulators.

3.0 EXPERIMENTAL RESULTS AND ANALYSES

3.1 DENSITY DISTRIBUTION IN SUPERSONIC BEAM

In the estimation of the dissociative attachment rate constant the density of Li_2 (v^*) has to be known. Our approach has been to monitor the depletion of Li_2 ($v = 0$) and use the known Franck-Condon factors for $B \rightarrow X$ decay to calculate the fraction of those molecules removed from $v = 0$ that ends up in a given excited vibrational level v^*. For an absolute estimate of Li_2 (v^*) density we therefore need to know the initial Li_2 ($v = 0$) density.

The Li_2 fraction in the beam is known from the initial equilibrium dimer to atom ratio in the lithium oven. Additional dimers form downstream of the slit nozzle, but we have tentative experimental evidence that these additional dimers remain vibrationally unrelaxed after formation, and hence do not contribute appreciably to the $v = 0$ population. This point is of somewhat academic interest in the 760°C to 820°C temperature/density range of the present experiments, where the dimer enhancement is only expected to be from 3 percent in the oven to ≈ 5 percent downstream. However the resolution of this issue by spectroscopic temperature measurements (Section 3.4) could be important for future work at 900°C, where the downstream dimer fraction could be 10 percent or more. The calculated Li_2 ($v = 0$) density will then depend strongly upon whether the downstream dimers are vibrationally relaxed, or not.

We require therefore to know the Li density in the experimental region, which is 10 cm downstream from the slit nozzle and 5 cm downstream from the skimmer. This number enters linearly into the dissociative attachment rate constant estimate.

In order to characterize the beam density distribution we measured the mass flow of Li at the chamber roof, 33 cm above the skimmer, by weighing the Li deposited on a thin stainless steel sheet in a 20 min exposure to the beam. This data was taken at 760°C oven temperature. The present density analysis will first be performed at this temperature and finally be extended to higher oven temperatures and beam densities. The data is shown in Figure 5 where the

3.0 EXPERIMENTAL RESULTS AND ANALYSES

3.1 DENSITY DISTRIBUTION IN SUPERSONIC BEAM

In the estimation of the dissociative attachment rate constant the density of Li_2 (v^*) has to be known. Our approach has been to monitor the depletion of Li_2 ($v = 0$) and use the known Franck-Condon factors for $B \rightarrow X$ decay to calculate the fraction of those molecules removed from $v = 0$ that ends up in a given excited vibrational level v^*. For an absolute estimate of Li_2 (v^*) density we therefore need to know the initial Li_2 ($v = 0$) density.

The Li_2 fraction in the beam is known from the initial equilibrium dimer to atom ratio in the lithium oven. Additional dimers form downstream of the slit nozzle, but we have tentative experimental evidence that these additional dimers remain vibrationally unrelaxed after formation, and hence do not contribute appreciably to the $v = 0$ population. This point is of somewhat academic interest in the 760°C to 820°C temperature/density range of the present experiments, where the dimer enhancement is only expected to be from 3 percent in the oven to ≈ 5 percent downstream. However the resolution of this issue by spectroscopic temperature measurements (Section 3.4) could be important for future work at 900°C, where the downstream dimer fraction could be 10 percent or more. The calculated Li_2 ($v = 0$) density will then depend strongly upon whether the downstream dimers are vibrationally relaxed, or not.

We require therefore to know the Li density in the experimental region, which is 10 cm downstream from the slit nozzle and 5 cm downstream from the skimmer. This number enters linearly into the dissociative attachment rate constant estimate.

In order to characterize the beam density distribution we measured the mass flow of Li at the chamber roof, 35 cm above the skimmer, by weighing the Li deposited on a thin stainless steel sheet in a 20 min exposure to the beam. This data was taken at 760°C oven temperature. The present density analysis will first be performed at this temperature and finally be extended to higher oven temperatures and beam densities. The data is shown in Figure 5 where the

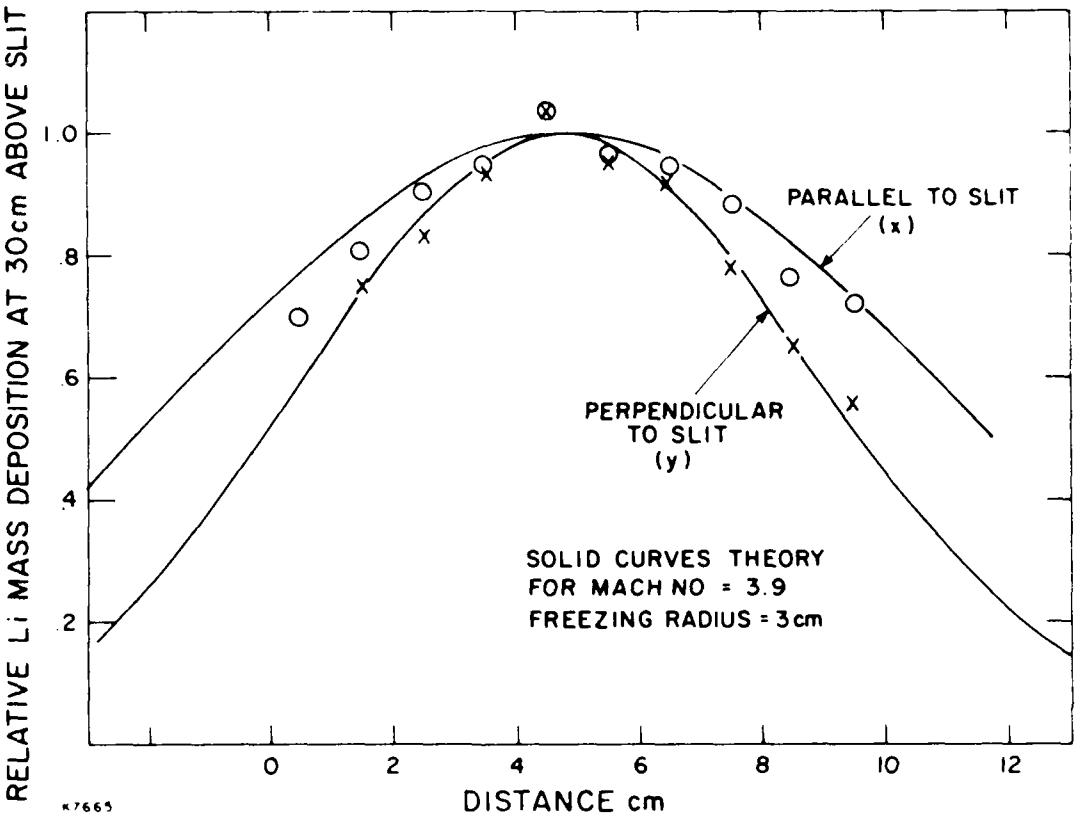

Figure 5 Measured and Fitted Li Deposition at 30 cm above Slit

relative mass distributions parallel and perpendicular to the slit are plotted. The total mass flow of Li was estimated by integrating the sample weighings over the entire collection area, and assuming that the Li which was weighed had formed either Li_3N or Li_2O in the laboratory air prior to weighing. The dark grey Li film was observed to turn light grey, and later greyish-white in the atmosphere. The following mass flows were observed at the center of the distribution:

Assumption	Mass Flow of Li
Pure Li	0.0028 g/cm^2/hr
Li_3N	0.0017 g/cm^2/hr
Li_2O	0.0013 g/cm^2/hr

Although it would clearly be possible to gain more precision either by weighing in an inert atmosphere, or by the use of different techniques (such as the change in resonant frequency of a crystal vibrator within the chamber), the above data is in accord to within ± 50 percent with the beam density model developed below.

The difficulty in modeling beam density downstream from the nozzle is caused by the existence of a transition from collisional fluid flow, or continuum flow, to free molecular flow which typically occurs several centimeters downstream in our experimental conditions. For all oven temperatures above 700°C the slit width (0.06 cm) is greater than the mean free path for Li-Li collisions (Figure 6) and hence we may use the continuum flow equations through the nozzle and immediately downstream.

$$\frac{\gamma}{\gamma-1}\frac{p}{\rho} + \frac{1}{2}\bar{u}^2 = \text{const.} \tag{3-1}$$

$$\rho\bar{u}A = \text{const.} \tag{3-2}$$

$$\frac{p}{p_0} = \left(\frac{\rho}{\rho_0}\right)^{\gamma} \tag{3-3}$$

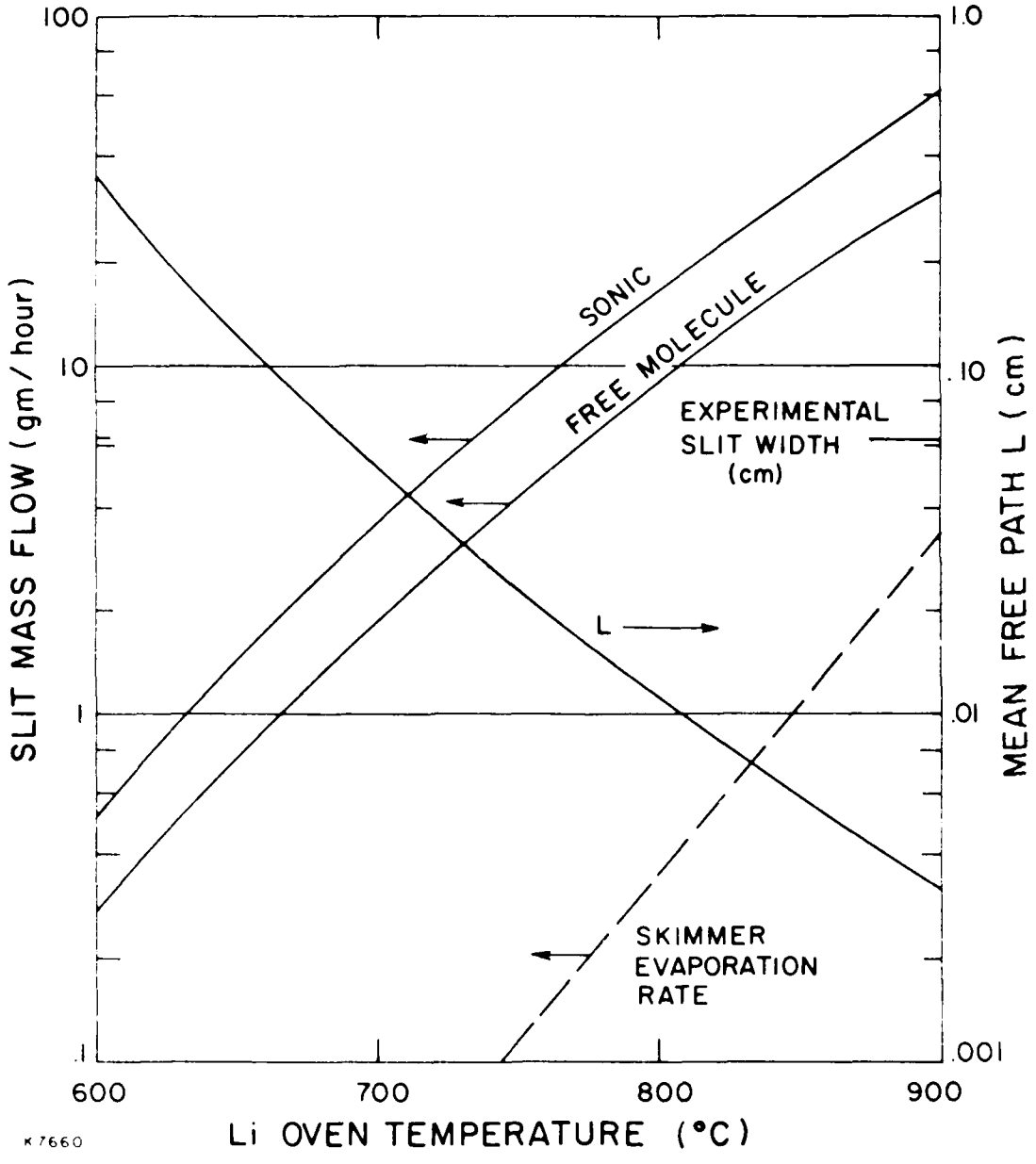

Figure 6 Mean Free Path and Mass Flow for Sonic and Free Molecular Flow

$$\bar{u} = Mu = M\sqrt{\gamma RT} \tag{3-4}$$

where P = pressure; ρ = mass density; $\bar{u}$ = mean velocity of flow; A = cross sectional area of flow; γ = ratio of specific heats (5/3 for Li); M = Mach number; T = temperature in flow and R = gas constant.

At the sonic point in the nozzle

$$T_s = \frac{2}{(\gamma+1)} T_0$$

where T_0 is the oven temperature, and in general

$$\rho = \rho_0 \left(\frac{T}{T_0}\right)^{\frac{1}{\gamma-1}} \tag{3-5}$$

$$T = \frac{T_0}{1 + \frac{(\gamma-1)M^2}{2}} \tag{3-6}$$

where ρ_0 is the oven Li density.

Firstly, the crude mass flow through the nozzle may be estimated by calculating ρ_s, $\bar{u}_s$ at the sonic point. This is shown in Figure 6 for our slit length of 1.9 cm and width 0.06 cm. For comparison, the lower free molecular flow rate is also shown, and should be applied for $T_0 < 760°$.

Secondly, an estimate may be made of the transition point to viscous flow by calculating the collision distance as a function of Mach number, which is shown in Figure 7 for oven temperatures of 760°C and 900°C. Dimension y, shown on Figure 7 is the beam width estimated from Eq. (3-2). We expect that free molecular flow begins when the collision distance is ~ 2 times the beam transverse dimension, giving a rough estimate of M = 3 for the transition point in the 760° oven case. In the plot of Figure 7 we have assumed a Li-Li collision sphere diameter of 2.5×10^{-8} cm.

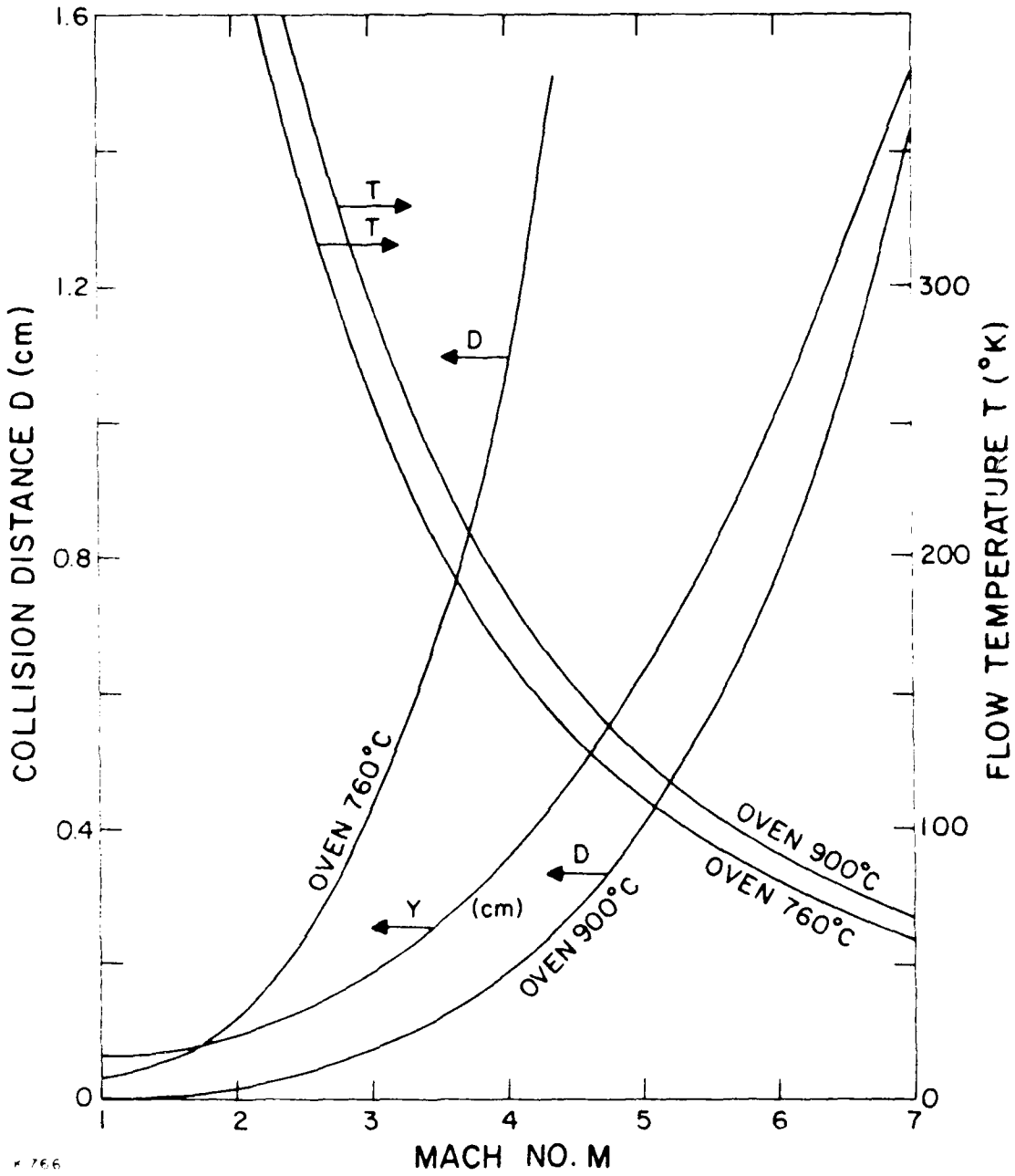

Figure 7 Collision Distance Compared to Beam Width y, and Flow Temperature

We define, rather arbitrarily, a 'freezing radius', r_F, as the radial distance from the slit nozzle at which the flow becomes collisionless. To estimate the density downstream from this point an integration of the free molecular flow has to be performed. This has been done numerically for the present experimental geometry and the results compared with the measured downstream flow rate and distribution. The geometry of the integration is illustrated in Figure 8. The skimmer aperture 'vignettes' the flow to a given point (x, y, z), and it is included as a constraint in the integration of all atoms leaving the cylindrical 'freezing surface'. The skimmer is 5 cm above the slit and its circular aperture has a diameter of 1.0 cm.

We use the velocity distribution at the freezing radius:

$$f\ (v_x,\ v_y,\ v_z) = \frac{\beta^3}{\pi^{3/2}} \exp\ [-\beta^2 \left\{ v_x^2 + v_y^2 + (v_z - v_o)^2 \right\}] \qquad (3.7)$$

where $\beta = \frac{1}{\sqrt{2RT}}$ and $v_o = \sqrt{\gamma RT}$

Additionally we use a $\cos^3\theta$ flux distribution on the freezing surface, where θ is the angle off axis in the y-z plane. This assumption is not critical to the result, as it approximates well to the free flow expected from a slit with M = 1 (Figure 9), which is itself an approximation to continuum flow. (For comparison, in Figure 9, the flux distribution for an M = 0 free flow case is also shown.)

The details of the free molecular flow integration procedure are lengthy but straightforward and will not be presented here. There are two variable parameters: the Mach number M and the freezing radius r_F. At a distance of 33 cm above the skimmer, which was the sample collection distance for the data of Figure 5, the computed x and y variations are different. The downstream pattern is oval-shaped with the long axis parallel to the nozzle slit. This is due to an effective imaging of the cylindrical freezing surface by the 'pinhole' of the skimmer aperture. It is found that the ratio of x- to y-dimensions of the distribution is very sensitive to the assumed freezing

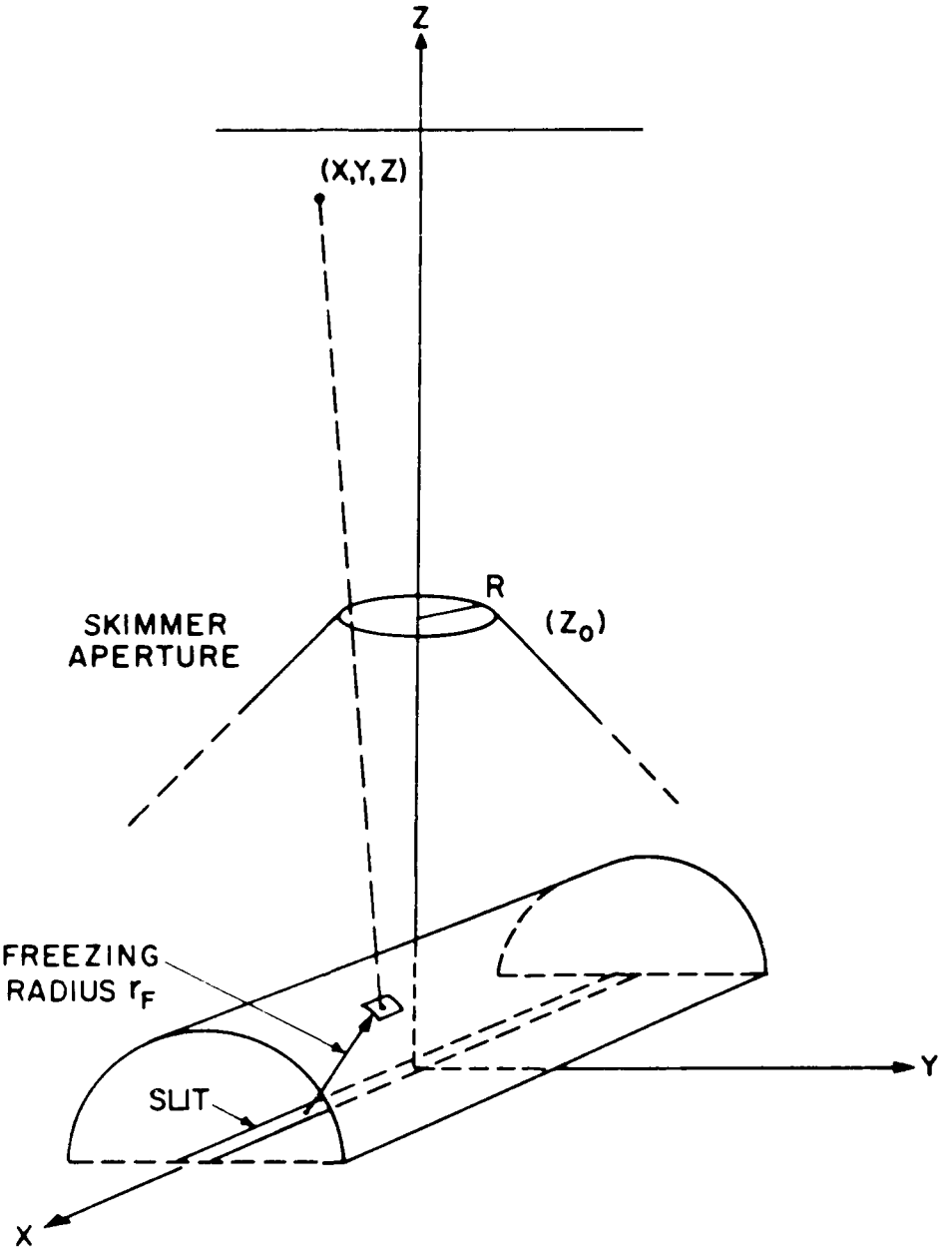

Figure 8 Geometry for Free Molecular Flow Integration

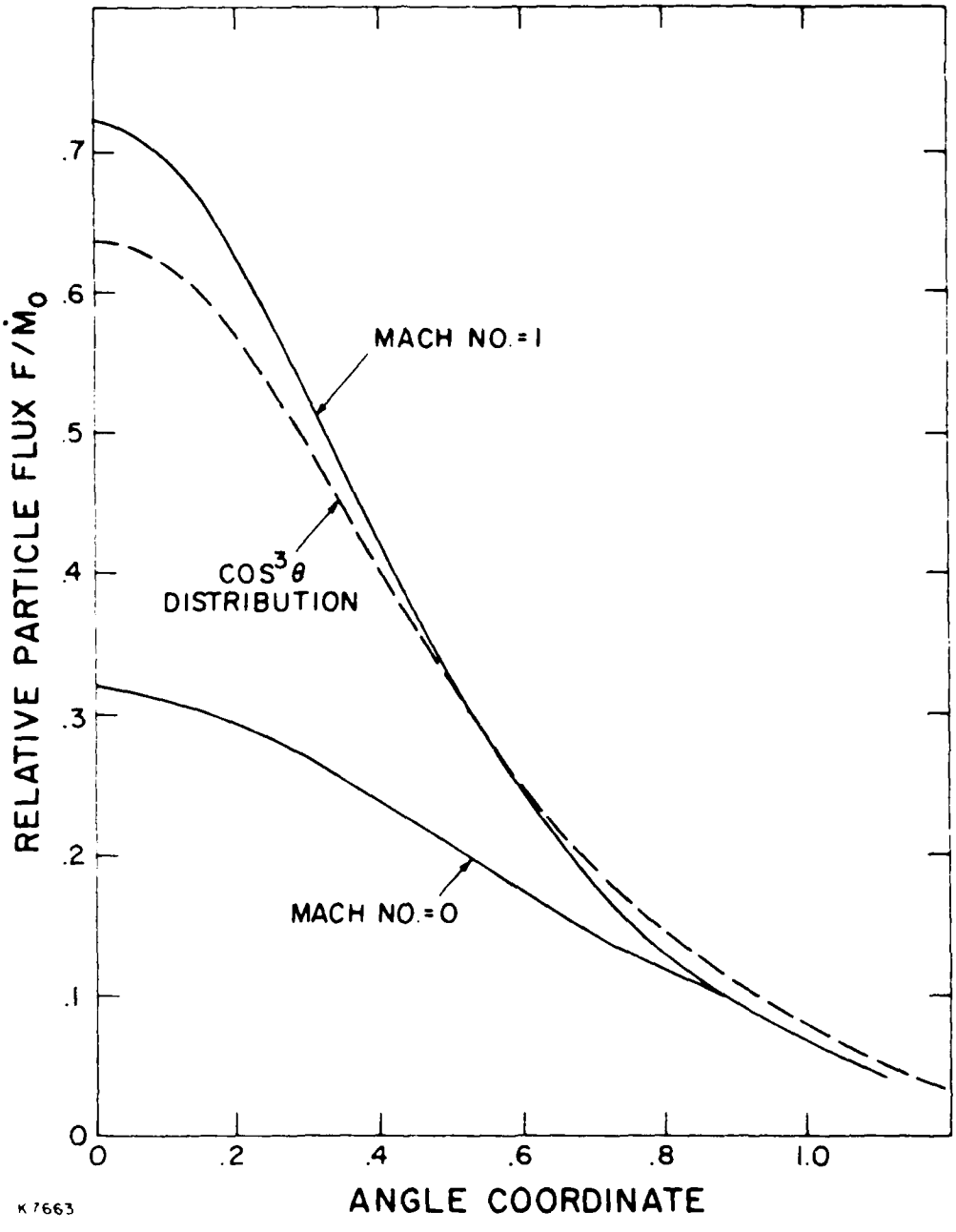

Figure 9 Angular Distributions for $\cos^3\theta$, Mach 1 and Mach 0 Flows

radius r_F. The Mach number M determines the overall size of the pattern, but does not affect the x- to y-dimension ratio. With this information a unique pair of $\{r_F, M\}$ may be found by fitting the computed distribution to the experimental data. This fit is shown in Figure 5 for the case $\{M = 3.9, r_F = 3.0$ cm$\}$, obtained for $T_o = 760°C$. For further information, the x-distribution dependence on M is computed in Figure 10.

This pair $\{M = 3.9; r_F = 3.0$ cm$\}$ at 760°C is reasonably consistent with the expectation for M and r_F obtained in the discussion above in reference to Figure 7.

For this pair of M and r_F the mean flux is computed to be 0.0026 g/cm^2/hr at the center of the sample plane 33 cm above the skimmer. This is to be compared with the measurement quoted above, particularly that obtained in the Li_3N assumption, 0.0017 g/cm^2/hr. When we allow for the slit having an effective width somewhat less than its true width, due to drag in the nozzle walls, the computed and measured flow rates are in respectable agreement. Because the effective width is not known accurately, all the data on density is presented for the full 0.06 cm slit width. However, in the use of this data for Li density estimation an effective width of 0.04 cm will be assumed.

We have used this combined flow model to predict experimental densities at 760°C as a function of position in the x-y plane at the experimental location 5 cm above the skimmer. Data along the z axis is shown in Figure 11, alongside the projection for free molecular flow commencing at the sonic surface. The x- and y-direction distributions at 10 cm are shown in Figure 12. In the experiments laser light was always incident parallel to the slit, i.e., in the x-direction. (Visually the fluorescence from the beam was also observed to extend over $\approx$ 3 cm.)

An approximation to the density behavior at higher oven temperature may be made by assuming a freezing radius $r_F = 3$ cm and M = 3.9, although in practice, as may be seen from Figure 7 the anticipated freezing radius increases at 900°C and with it the Mach number. The use of M = 3.9 with $r_F = 3.0$ cm at increasing T_o, p_o generates the data of Figure 13 in the experimental region, showing that densities of $> 6 \times 10^{13}$ cm^{-3} are available at our operating limit of 900°C. This will be a lower limit because the Mach number and freezing radius will actually be larger at this temperature, and the beam more directional.

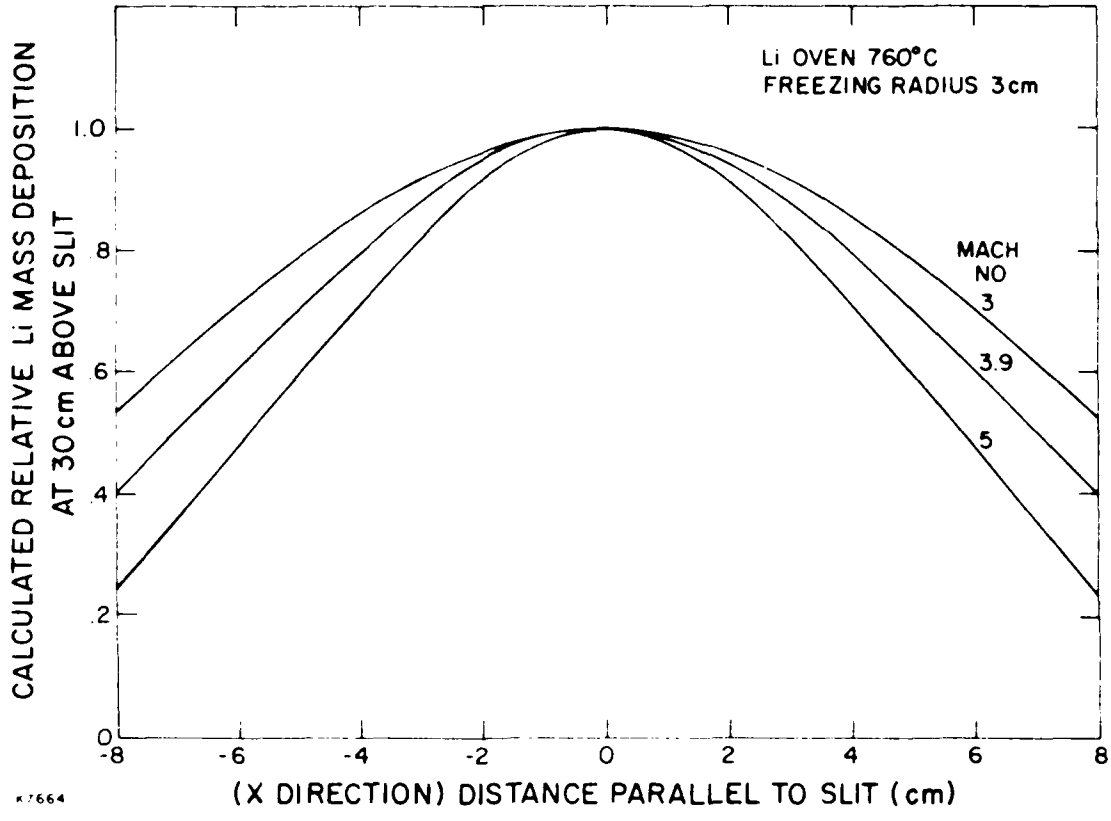

Figure 10 Dependence of Li Deposition in X direction as a Function of Mach Number

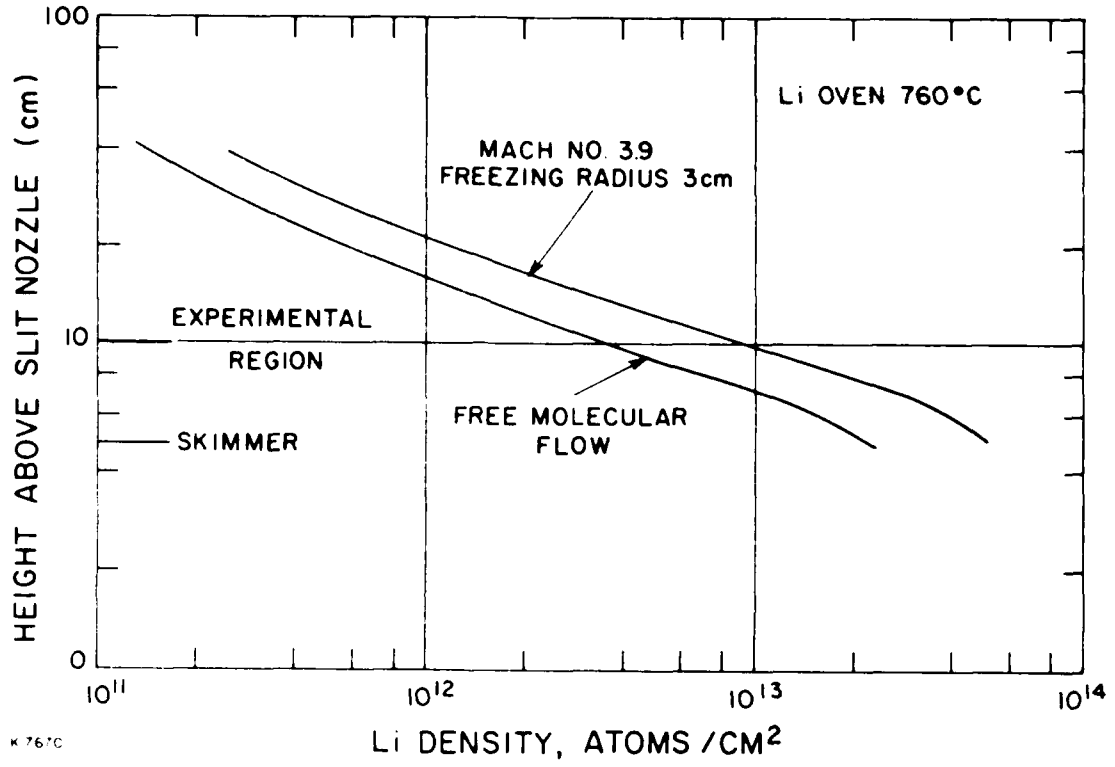

Figure 11 Calculated Li Density as a Function of Height Above Slit Nozzle

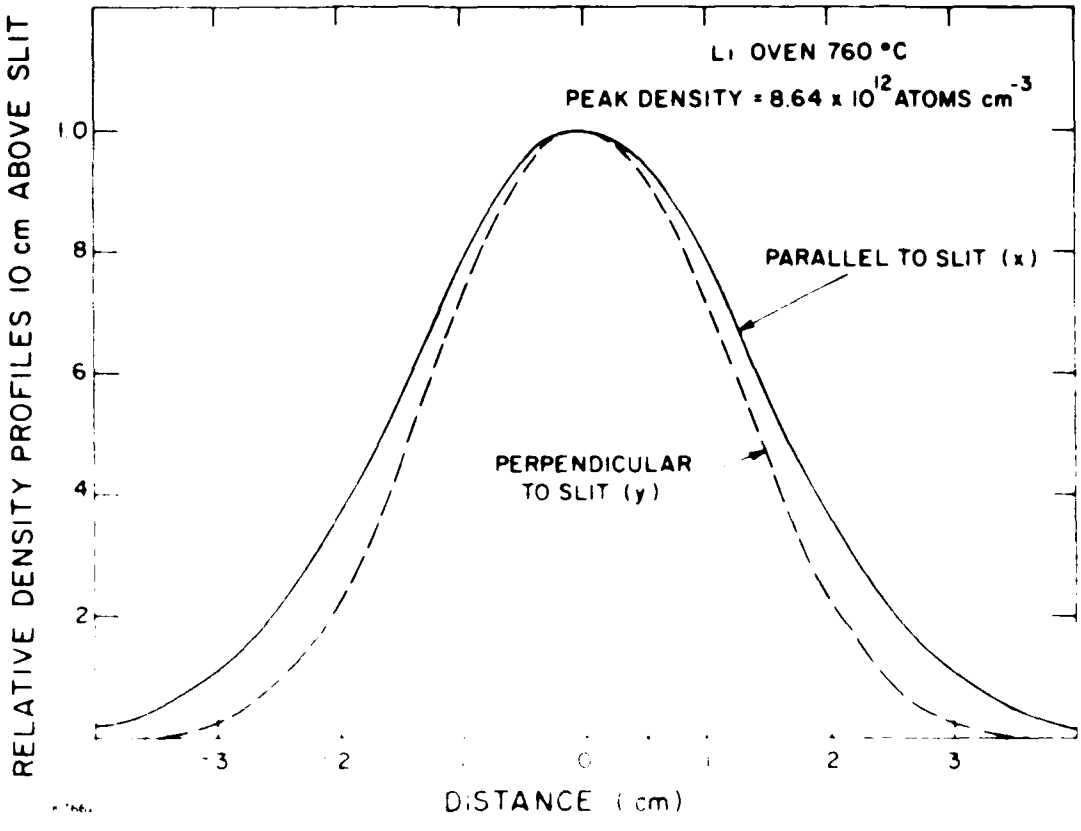

Figure 12 Calculated [illegible] cm Above Slit

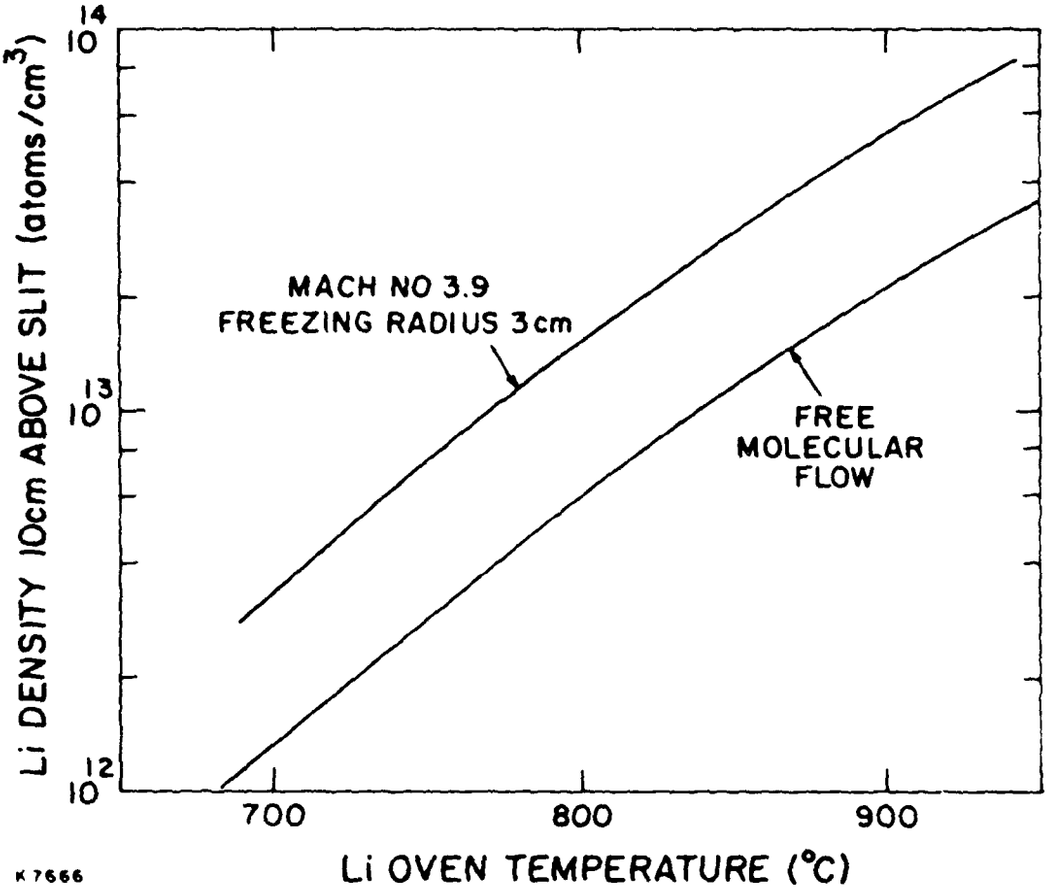

Figure 13 Calculated Li Density 10 cm Above Slit as a Function of Li Oven Temperature

3.2 Li^+ MEASUREMENTS: EFFICIENCY OF COLLECTION

With reference to Figure 3 photo-ions are created in the cylindrical volume where the photoionization laser beam intersects the Li beam. After a variable delay a pulsed voltage of up to 2.2 kV is applied to the extraction plate and ions are impelled into the flight tube through a 90 percent transparent mesh. Because they start at the mid-plane between the extraction electrodes their maximum energy is only 1.1 keV. The measured ion current increases with extraction voltage as shown in Figure 14. The increase in collection efficiency with extraction voltage is due to a combination of effects:

1. The magnetic field section of the drift tube suppresses electrons when negative ions are being measured, but also deflects the positive ions by a voltage-dependent amount so that they can partly miss the collector plate.
2. The cylindrical plasma undergoes a rapid radial expansion due to the plasma pressure and the perpendicular velocity components can reduce the ion collection efficiency.
3. These are possible effects from space-charge limited current flow (a) at the surface of the plasma and (b) in the flight tube.
4. The ions are created in a supersonic Li beam which has a velocity of $\approx 2 \times 10^5$ cm/sec^{-1} perpendicular to the flight tube. The angles of the ion paths depend on the extraction voltage.

These four effects will be further discussed in turn:

1. The magnetic field section contains a 200 G field transverse to the tube over a length of 4 cm at a position 10 cm in front of the collector plate (diameter 2.5 cm). The ion gyroradius is $R = vM_i/qB$ where q is the ion charge. The deflection angle is $\theta = 4/R$ rads if R is expressed in centimeters. At the maximum extraction voltage R = 62 cm, $\theta = 0.06$ rads and almost all the ions are collected. At an extraction voltage of 60 V none of the ions can reach the plate. This effect is plotted in Figure 15.
2. The plasma expands at a velocity close to the ion acoustic velocity $\sqrt{kT_e/M_i}$ where T_e is the electron temperature. The details of the radial velocity profile are calculated in Section 3.3, and the

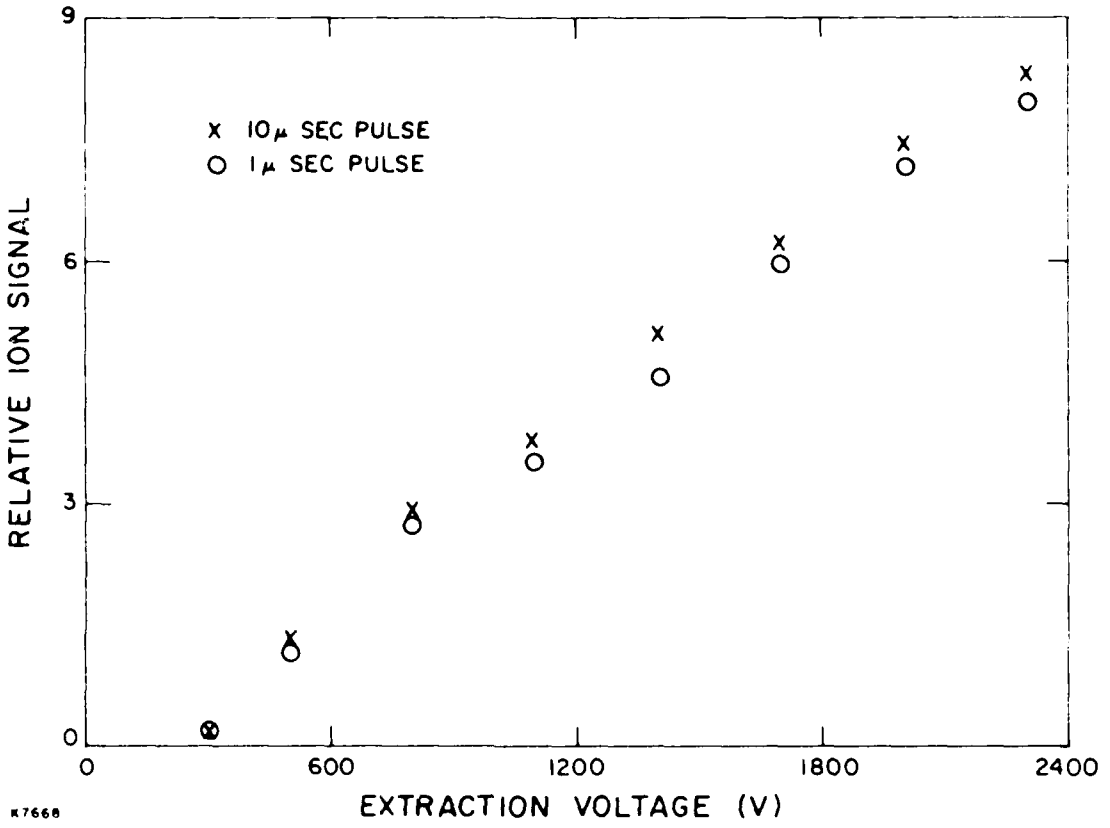

Figure 14 Measured Li^+ Signal as a Function of Extraction Voltage

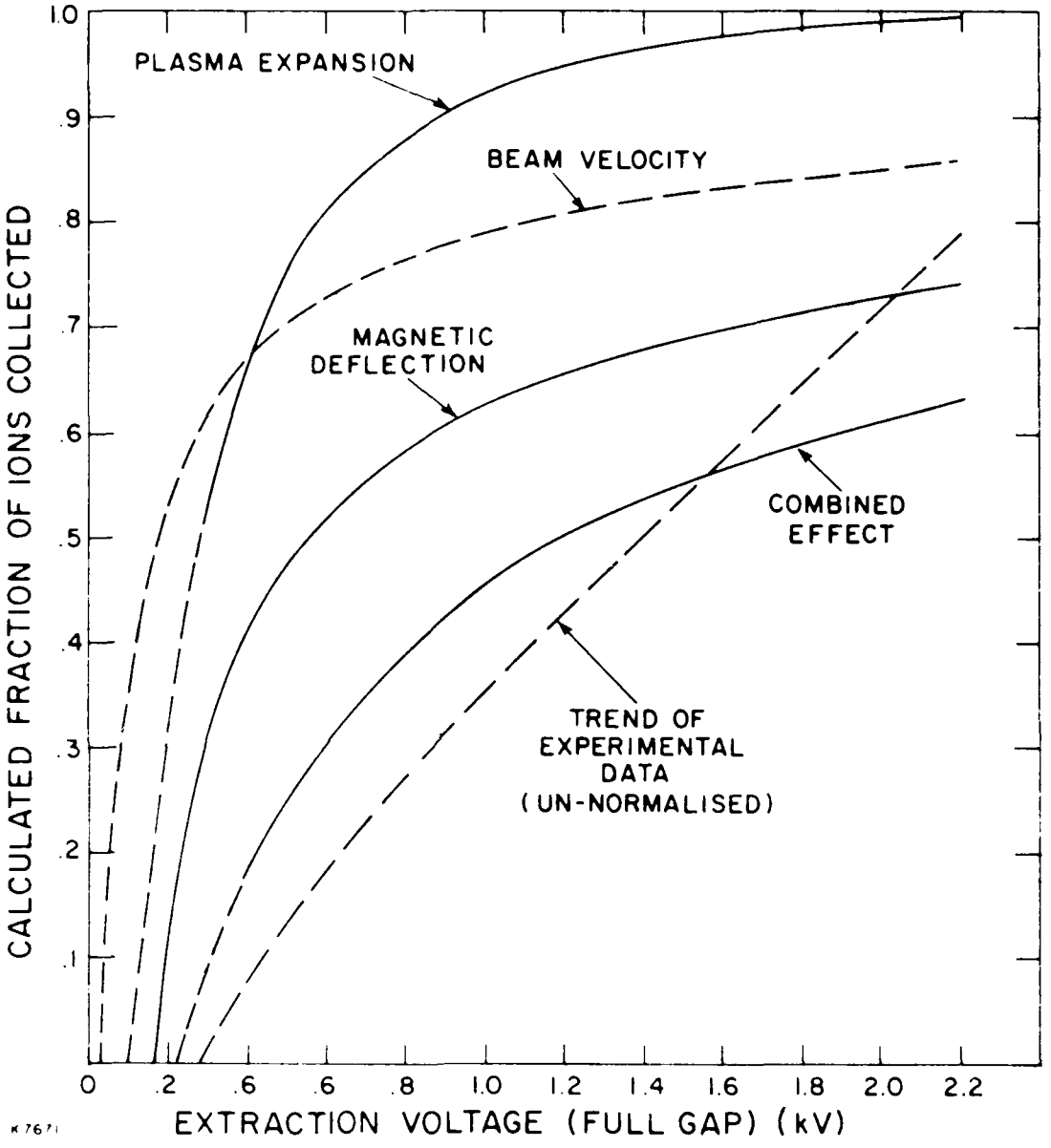

Figure 15 Factors Influencing Ion Collection Efficiency

effect on the ion collection efficiency has been calculated numerically, using the output from the plasma expansion computation. This effect is plotted in Figure 15, where it may be seen to be smaller than the magnetic field effect in the conditions of this experiment.

3. Space charge was shown to be a small effect experimentally by varying the extraction pulse between 1 μsec and 10 μsec (Figure 14), when no difference in ion current was recorded. If the ions had been incompletely extracted due to space-charge limited current flow in 1 μsec, then an increased signal should have been observed at 10 μsec. As to the effect of space charge repulsion in the drift tube, this can be shown to be negligibly small by calculation.
4. At the maximum extracted ion energy of 1.1 keV, the Li^+ velocity is 1.7×10^7 cm/sec^{-1}, implying a 1.4 μsec transit time in the flight tube. The supersonic beam velocity of 2×10^5 cm/sec^{-1} imposes an angle of 0.012 rad on the beam, leading to a displacement of 0.3 cm at the 24 cm distant collector plate. The effect of reducing the extraction voltage is to eventually cut all ions off due to this angle increasing. This effect is plotted in Figure 15.

In conclusion, the combined effects of items 1 through 4 above lead to a predicted ion current dependence rather similar to that observed in the experiment. The comparison is made in Figure 15 where it may be seen that the experimental data rises more rapidly than the calculated curve for the combined effect. The difference at high voltages might be accounted for by secondary electron production at the surface of the collector plate, which effectively enhances the ion current. We use this analysis to calculate a Li^+ ion collection efficiency of 63 percent in our experimental conditions, which is reduced to 57 percent when the 90 percent transmission mesh is included. The same number applies to Li^- collection.

The dependence of the Li^+ signal on the Li over vapor pressure is shown in Figure 16. (Data taken at an extraction voltage of 2.2 kV.) The dip in signal below a Li pressure of 1 torr occurs at the transition region from continuum flow to the molecule flow which occurs at ≈ 700°C. Below this temperature the Li mean free path is greater than the slit width, as illustrated in Figure 6, and the downstream beam density drops substantially. The same

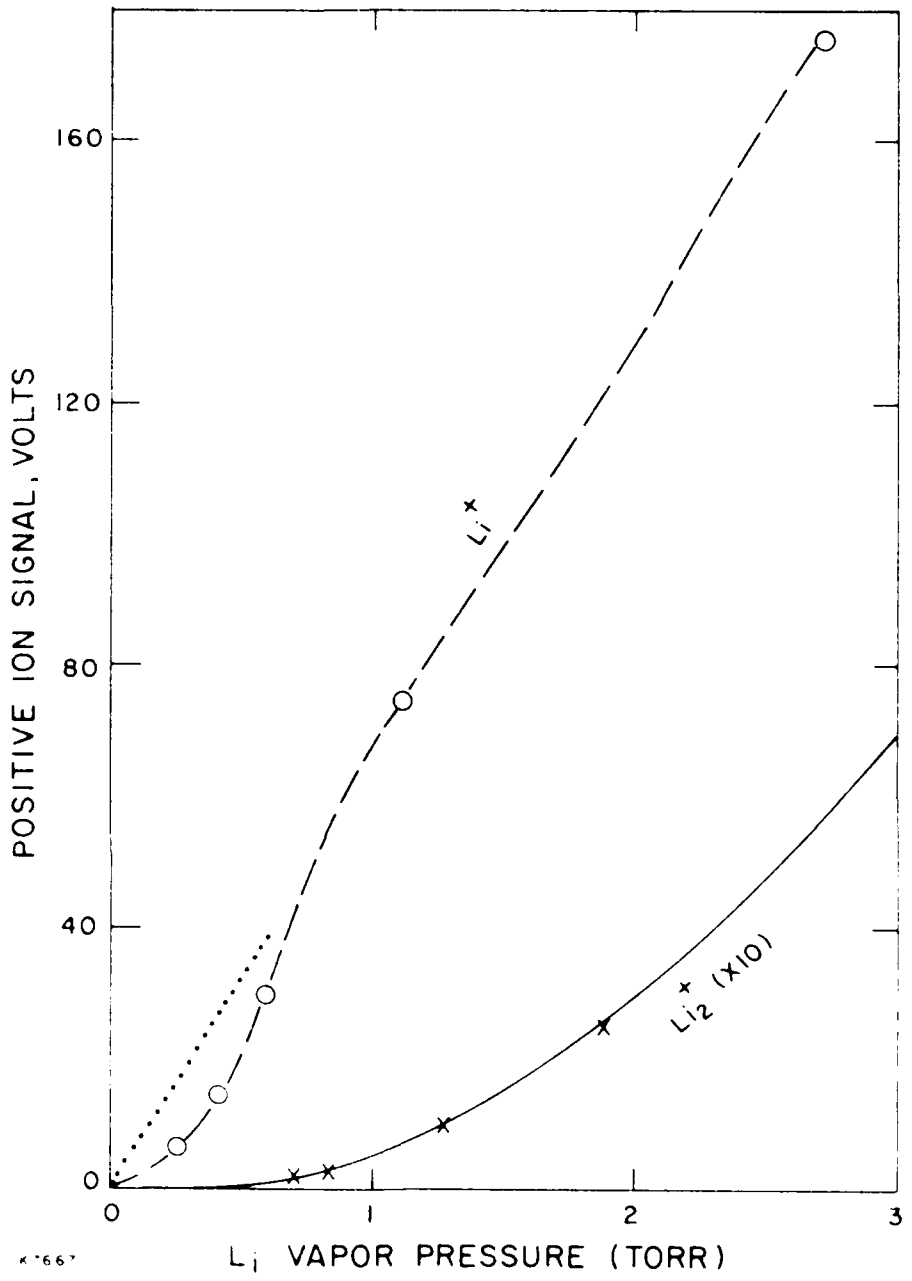

Figure 16 Dependence of Li^+, Li_2^+ Signals on Li Vapor Pressure in Oven

Li^+ data is plotted on a logarithmic plot as a function of 1/T in Figure 17. Here it may be seen that the Li^+ signal follows the Li oven density at temperatures above $\approx 700^\circ C$.

Given the Li beam density and the excitation laser geometry and intensity an estimate can be made of the number of Li^+ ions to be expected. The photoionization scheme is illustrated in Figure 18. The 610 nm line is more intense than the 671 nm line because the dye is more efficient, and hence the third step is predominantly at 610 nm (assuming that the photoionization cross section depends only weakly on wavelength). The laser intensities are such that both the $^2S - {}^2P$ and $^2P - {}^2D$ transitions are saturated during the 5 nsec laser pulse. The photoionization step, which has a cross section of $\approx 3 \times 10^{-17}$ cm^2[3] is not saturated. As a first approximation the populations of the ^2S, ^2P and ^2D states are pumped until they reach the ratio of their degeneracies. A more detailed picture includes radiative losses from the ^2D state to states other than the ^2P.

The Li transitions are Doppler-broadened with a full linewidth of 3.0 GHz at the $\approx 150^\circ K$ beam temperature. The lasers have a 0.25 Å bandwidth ($\sim$ 18 GHz). The stimulated emission rate can be shown to depend only on the laser intensity and the spontaneous emission rate for the transitions. Labelling the $^2S - {}^2P$, $^2P - {}^2D$ and ^2D-ion transitions 1, 2, 3 respectively, then their stimulated emission rates are

$$\begin{aligned} \Gamma_1 &= 710\, E_1 && (5\ \text{nsec})^{-1} \\ \Gamma_2 &= 3000\, E_2 && (5\ \text{nsec})^{-1} \\ \Gamma_3 &= 0.1\,(E_1 + E_2) && (5\ \text{nsec})^{-1} \end{aligned} \qquad (3\text{-}6)$$

in which E_1 and E_2 are the laser energies (in mJ/cm^2) delivered to the atoms and the unit of time is the 5 nsec laser pulse duration. The degeneracies of levels ^2S, ^2P and ^2D are 4, 6 and 10, respectively. If we denote these states by number 0, 1, 2 and the ion by 3, then equations may be written for the state populations:

3. 'Photionization of Excited Rare Gas Atoms', Duzy, C. and Hyman, H.A., Phys. Rev. A 22, 1878 (1980).

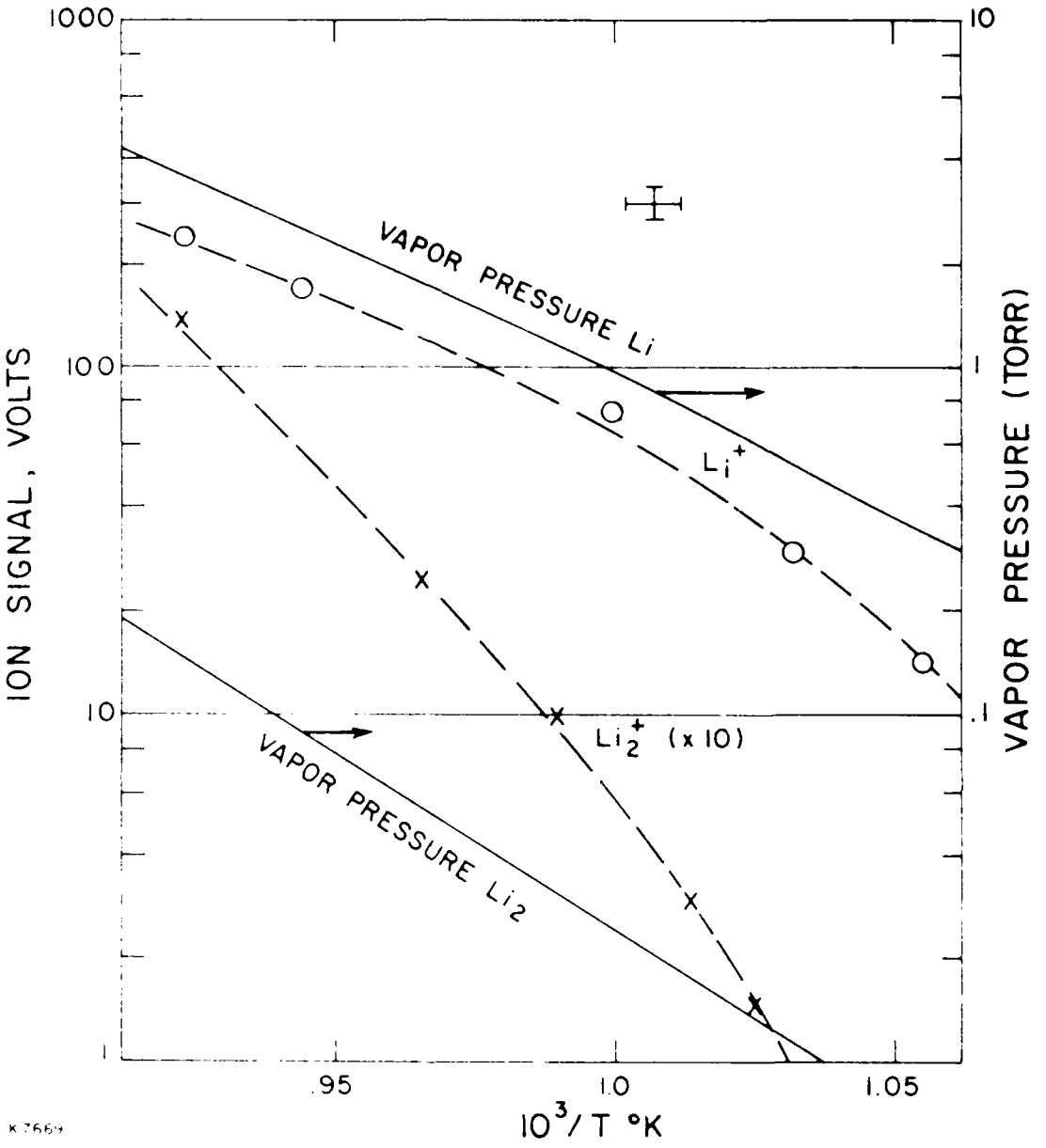

Figure 17 Plots of Li, Li_2^+ Ion Signals Against 1/T

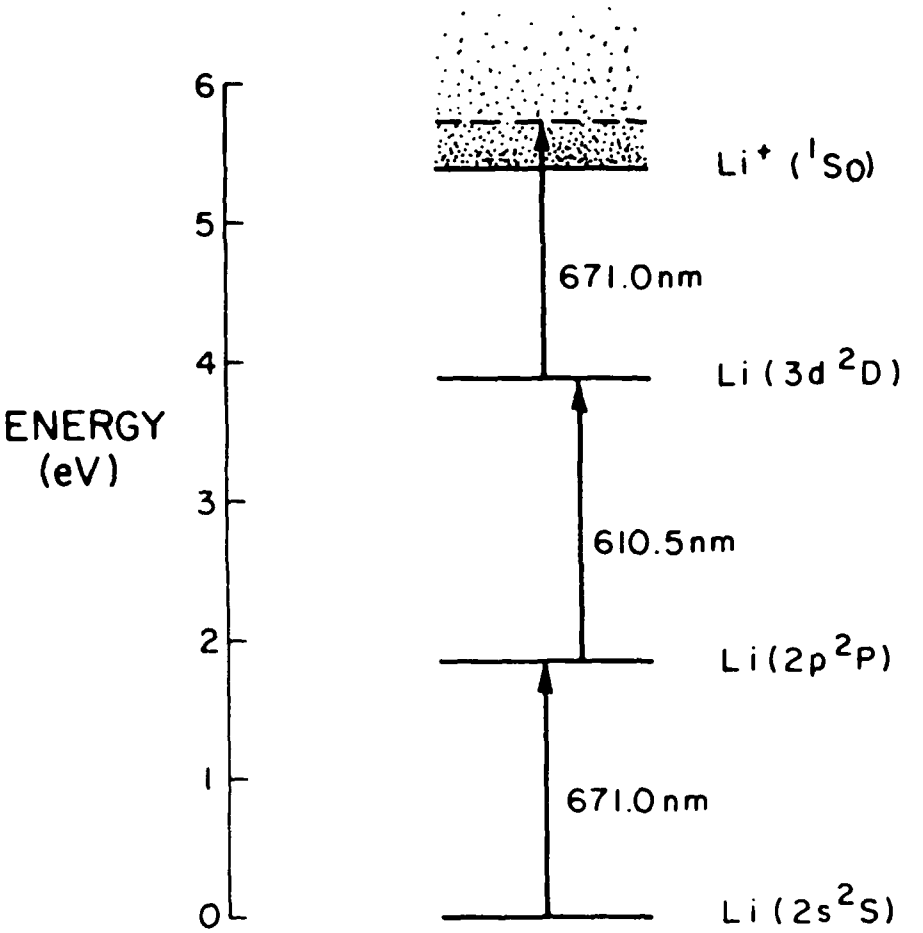

Figure 18 Three-Step Photoionization of Li

$$\dot{n}_0 = -n_0\Gamma_1/q_0 + n_1(\Gamma_1 + R_1)/q_1$$

$$\dot{n}_1 = n_0\Gamma_1/q_0 - n_1(\Gamma_1 + R_1 + \Gamma_2)/q_1 + n_2(\Gamma_2 + R_2)/q_2$$

$$\dot{n}_2 = n_1\Gamma_1/q_1 - n_2(\Gamma_2 + \Gamma_3 + R_2 + R_3)/q_2 \qquad (3\text{-}9)$$

$$\dot{n}_3 = n_3\Gamma_3/q_2$$

in which R_1, R_2 and R_3 are the spontaneous decay rates of states 1, 2 and 3, in time units of 5 nsec. We have used the values of $\{R_1 = 0.1; R_2 = 0.65; R_3 = 0.65\}$. As mentioned above the degeneracies are $\{q_0 = 4, q_1 = 6, q_2 = 10\}$.

Integrating the above equations numerically we obtained the following table of data for the fraction of Li atoms ionized to $Li^+ + e^-$:

E_1 (mJ cm^{-2})	E_2 (mJ cm^{-2})	Fraction Ionized
0.01	0.01	0.00005
0.03	0.03	0.00023
0.1	0.1	0.00092
0.3	0.3	0.00289
1	1	0.00972
3	3	0.0291
10	10	0.093
30	30	0.254
100	100	0.599

In the experiments of 5 μJ pulse was incident at 610 nm and a 2 μJ pulse at 670 nm, into a cylinder of radius 0.1 cm. Assuming uniform intensity this gives a fractional ionization of 1.0×10^{-3}. At 760°C Li oven temperature the experimental beam density was 9×10^{12} Li atm/cm^{-3} and hence we estimate a production of 2.8×10^{8} Li^+ ions/cm of the laser beam. Ions are

collected with a calculated 57 percent efficiency (see above) and from a 2.5 cm length of the laser beam. The net predicted charge collected per pulse is therefore 6.4×10^{-11} Coul. The measured charge is somewhat less than this, namely 2×10^{-12} Coul.

At the present time we do not know where to attribute this discrepancy between calculated and measured ion current. One possibility is that the photoionization cross section is less than the 3×10^{-17} cm^2 theoretical estimate.[3] However it is not likely to be $< 1 \times 10^{-17}$ cm^2. It is more likely that the presence of a cylindrical plasma between the extraction plates is distorting the extraction field, and hence spreading the ions into larger angles. Because the plasma disappears during the extraction pulse this is a time-dependent effect.

3.3 MODELLING OF PLASMA EXPANSION

In a Li vapor density of 10^{12} to 10^{14} cm^{-3} a photoionization laser pulse creates a fractional ionization of 10^{-3} to 10^{-2} throughout the laser beam volume. In the present experiments this volume is a cylinder of radius ≈ 0.1 cm and length ≈ 3 cm. Under the pressure of the electron gas this plasma expands radially at a velocity of the order of the ion acoustic velocity. As it expands the electron temperature is cooled adiabatically. The timescale of expansion is so fast ($\approx 10^{-6}$ sec) that the electrons lose negligible collision energy to either the ions or the neutrals, but expend almost all their energy on radial acceleration of the ions. Because the Li beam is cold and has a density $\lesssim 10^{14}$ cm^{-3} the ions are created at temperatures $\lesssim 150^{\circ}K$ and do not on average collide with Li atoms during the expansion. The electron and Li^+ plasma therefore expands as if the neutral atoms were not there at all.

To verify these assertions let us review the rates for collisional relaxation of the electron energy at $n_e = 10^{10}$ cm^{-3}, the electron density for the results to be discussed.

1. Electron-Electron Relaxation

The electron-electron energy relaxation time is

$$t_{ee} = \frac{11.4\ T_e^{3/2} A_e^{1/2}}{n_e \ln \Lambda} \text{ sec} \qquad (3\text{-}10)$$

For our case the electron temperature T_e = 6005°K (≡ 0.52 eV), A_e = 1/1823, $\ln\Lambda \approx 10$, giving

$$t_{ee} = \frac{1.24 \times 10^4}{n_e} \text{ sec} \tag{3-11}$$

Therefore at $n_e = 10^{10}$ the electron energy distribution relaxes from the δ-function photoionization distribution to a Maxwellian of the same average energy in a characteristic time of 1.24 μsec.

2. Electron-Ion Relaxation

The electron-ion energy relaxation time is

$$t_{e+} = \frac{5.87}{n_e \ln\Lambda} \frac{A_e A_+}{z_+^2} \left(\frac{T_e}{A_e} + \frac{T_+}{A_+} \right)^{3/2} \text{ sec} \tag{3-12}$$

where A_+ = mass number of Li^+ = 7
A_e = 1/1823
z_+ = charge of Li^+ = 1
T_e = electron temperature = 6005°K
T_+ = ion temperature $\lesssim$ 150°K

whence $t_{e+} = \frac{8.2 \times 10^7}{n_e}$ sec,

and at $n_e = 10^{10}$, negligible ion heating occurs in 10^{-6} sec.

3. Electron-Neutral (atom or molecule) Relaxation

The cross sections for momentum transfer are:[4,5]

4. 'Absolute Total Cross Sections for the Scattering of Low-Energy Electrons by Lithium Atoms,' Jaduszliwer, Tino, A., Bederson, B., and Miller, T.M., Phys. Rev. A, 24, 1249 (1981).

5. 'Measurements of Total Cross Sections for Electron Scattering by Li_2 (0.5 - 10 eV),' Miller, T.M., Kasdan, A. and Bederson, B., Phys. Rev. A 25, 1777 (1982).

Electron Energy (eV)	σ (Li) ($\AA^2$)	σ (Li_2) ($\AA^2$)
0.5	$\approx$ 200	541
1.0		307
2.0	115	199
4.0	88	
10.0	72	

The characteristic cooling time of electrons through elastic collisions with neutrals of mass m_n is

$$t_n \approx \frac{m_n}{2m_e n_n v\sigma} \tag{3-13}$$

where n_n is the neutral density and v is the electron velocity.

For e^- - Li relaxation we find $t_n \approx 10^{-4}$ sec at $n_{Li} \approx 10^{13}$ cm^{-3}, whereas for e^- - Li_2 relaxation, assuming 8 percent dimer we find $t_n \approx 10^{-3}$ sec. Neither of these processes are significant on the 10^{-6} sec timescale of plasma expansion.

Reviewing items 1, 2 and 3 therefore, we conclude that the electrons may develop into a Maxwellian distribution in $\approx 10^{-6}$ sec, but their only significant energy loss on this timescale is the work done on expanding the plasma.

The equations of continuity and conservation of energy and momentum may be written for an axially symmetric problem as

$$\frac{d\rho}{dt} = \frac{\rho}{r} \frac{\partial(vr)}{\partial r} \tag{3-14}$$

$$\rho \frac{dv}{dt} = - \frac{\partial p}{\partial r} \tag{3-15}$$

$$\rho \frac{d\epsilon}{dt} = - \frac{p}{r} \frac{\partial(vr)}{\partial r} \tag{3-16}$$

where ρ is the mass density of the plasma

p is the internal pressure

v is the velocity of radial motion of the plasma

r is the radial position coordinate

ϵ is the internal energy per unit mass of the plasma

The ions are cold, so that the equation of state is

$$p = \frac{\rho}{m_i} k T_e \tag{3-17}$$

where m_i is the ion mass and T_e is the electron temperature.

Also in this case $\epsilon = 3kT_e/2m_i$, so that $\epsilon = 3p/2\rho$.

We were unable to find an analytical integration procedure for this set of equations, so a numerical integration was performed, using a second order accurate difference scheme. A Lagrangian approach was adopted, with a division of the plasma into 40 radial zones, whose boundaries moved with the ions. To ensure energy conservation the electron energy was re-computed each time step by subtraction of the computed average ion kinetic energy from the initial electron energy.

The initial distribution of the plasma density was taken as a Gaussian, which was a good representation of the experimental case.

The computed evolution of the plasma showed regularities which indicated that a good analytical approximation could be made. Firstly, the radial density distribution remained Gaussian, but with an expanded radial scale. Secondly, the ion velocity at all times was linearly dependent on the radius. Thirdly, as expected, the ions reached a final asymptotic velocity distribution controlled by the initial energy of the electrons. It was found that the following set of equations described the numerical solution to an accuracy of ≈ 5 percent in a wide range of cases:

$$r = r_o (\gamma t + e^{-\gamma t}) \tag{3-18}$$

$$\rho = \frac{Nm_i}{\pi r_e^2(t)} e^{-\frac{r^2}{r_e^2(t)}} \tag{3-19}$$

$$v = r_o \gamma \left(1 - e^{-\gamma t}\right) \tag{3-20}$$

where r is the position at time t of a particle initially at $r = r_o$, and

$$\gamma = \frac{1}{r_{eo}} \sqrt{\frac{2\epsilon_o}{m_i}} \tag{3-21}$$

where r_{eo} is the initial 1/e density radius, ϵ_o is the initial electron energy and m_i the ion mass. In the expression for ρ, N is the total number of ions per unit length of the cylindrically symmetric plasma and

$$r_e(t) = r_{eo} \left(\gamma t + e^{-\gamma t}\right) \tag{3-22}$$

is the position of the 1/e density radius at time t.

Substituting for r_o in the expression for v we obtain

$$v = c(t)r \tag{3-23}$$

$$\text{with } c(t) = \frac{\gamma \left(1 - e^{-\gamma t}\right)}{\left(\gamma t + e^{-\gamma t}\right)} \tag{3-24}$$

which expresses the linear dependence of velocity upon radius at time t.

Although the above set of equations describes the numerical solutions to 5 percent accuracy, they do not apparently form an exact solution set to the expansion equations. Further work is needed to verify this point.

In the estimation of dissociative attachment rate constants it is necessary to compute the duration for which the electron energy exceeds the dissociative attachment threshold energy. At late times the electrons become very cool due to their loss of energy into ion radial motion. The electron energy at a given time may be shown to be

$$\epsilon_e(t) = \epsilon_0 \, e^{-\gamma t} \, (2 - e^{-\gamma t}) \tag{3-25}$$

For a dissociative attachment threshold energy of ϵ_{DA} the time t_{DA} at which $\epsilon_e(t) = \epsilon_{DA}$ is given by

$$t_{DA} = -\frac{1}{\gamma} \, n \left[1 - \sqrt{1 - \frac{\epsilon_{DA}}{\epsilon_0}} \right] \tag{3-26}$$

For example, when the electron initial energy is $\epsilon_0 = 0.53$ eV and $r_{e0} = 0.1$ cm is the initial 1/e plasma radius, a dissociative attachment threshold of $\epsilon_{DA} = 0.25$ eV implies $t_{DA} = 0.34$ μsec.

The plasma expansion therefore limits the time available for dissociative attachment to occur in the present experiment. The implications of this for experimental sensitivity are discussed below.

Plasma expansion is also one of the causes of reduced ion collection efficiency when the extraction voltage is less than its 2.2 kV maximum (see Figure 15). The expansion of the extracted ions continues down the flight tube. The effect of this on ion collection efficiency has been modeled numerically, using the computed radial ion velocities and projecting them, with appropriate density weighting, onto the collector plate. The results, shown in Figure 15 show that plasma expansion accounts for at least part of the reduction in collected ions at reduced voltage. The remainder may be accounted for by other effects as discussed in Section 3.2 above.

3.4 Li_2^+ MEASUREMENTS: TEMPERATURE ANALYSIS

A Li_2^+ ion signal is observed when the Li_2 (B - X) transition is pumped with a single blue dye laser. This two-step photoionization process is illustrated schematically in Figure 19. The same process has previously been observed in experiments where a hot, effusive Li beam has been irradiated with an Argon ion laser.[6] The present experiment is thought to be the first in which a supersonic Li beam was involved. Because of the very cold temperatures in the beam unusually clear spectra have been recorded in which the vibrational bands are clearly separated from each other and also from the minority $^6Li^7Li$ spectrum (Li consists of 94 percent ^7Li and 6 percent ^6Li). We have tuned the blue laser (bandwidth 0.25 Å) over the range 450 nm to 480 nm to obtain the Li_2^+ spectrum corresponding to first step excitations on the Li_2 (B - X) 7-0 down to 3-0 transitions.

In this spectrum the contribution from the $v = 1$ Li_2 (X) state is relatively small compared to the $v = 0$ contribution, indicating that the vibrational relaxation of Li_2 into the $v = 0$ state is > 90 percent complete in this expansion.

In Figure 17 the Li_2^+ signal is displayed as a function of Li oven temperature. For this measurement the blue laser was tuned to the maximum of the 0-5 band, at 4617.7 Å. We note that the Li_2^+:Li^+ signal ratio increases more rapidly than the Li_2:Li equilibrium ratio over this temperature range, an effect which is principally due to the reduction in rotational temperature which occurs at high beam densities. This causes a more dense population of the J = 4, 5, 6 levels (near the band head) which are effectively the levels monitored in this particular measurement. A more detailed look at the Li_2^+:Li^+ ratio in the 740°C to 790°C oven temperature range showed that the signal ratio was tending to reproduce the Li_2:Li ratio much more closely.

The Li_2 rotational temperature was estimated by comparing the measured rotational structure on a band with that computed for different thermal distributions of rotational states. In Figure 20 the Li_2^+ signal from the 0-6 band is shown for an Li oven temperature of 800°C. The computed 0-6 band shapes for 100°K and 150°K are shown in Figure 21 and Figure 22. In these calculations the relative strengths of the P, Q and R branches were computed

6. 'Isotope Fractionation in Two-Step Photoionization of Li_2,' Rothe, E.W. and Mathur, B.P., Chem. Phys. Lett. 53, 74 (1978).

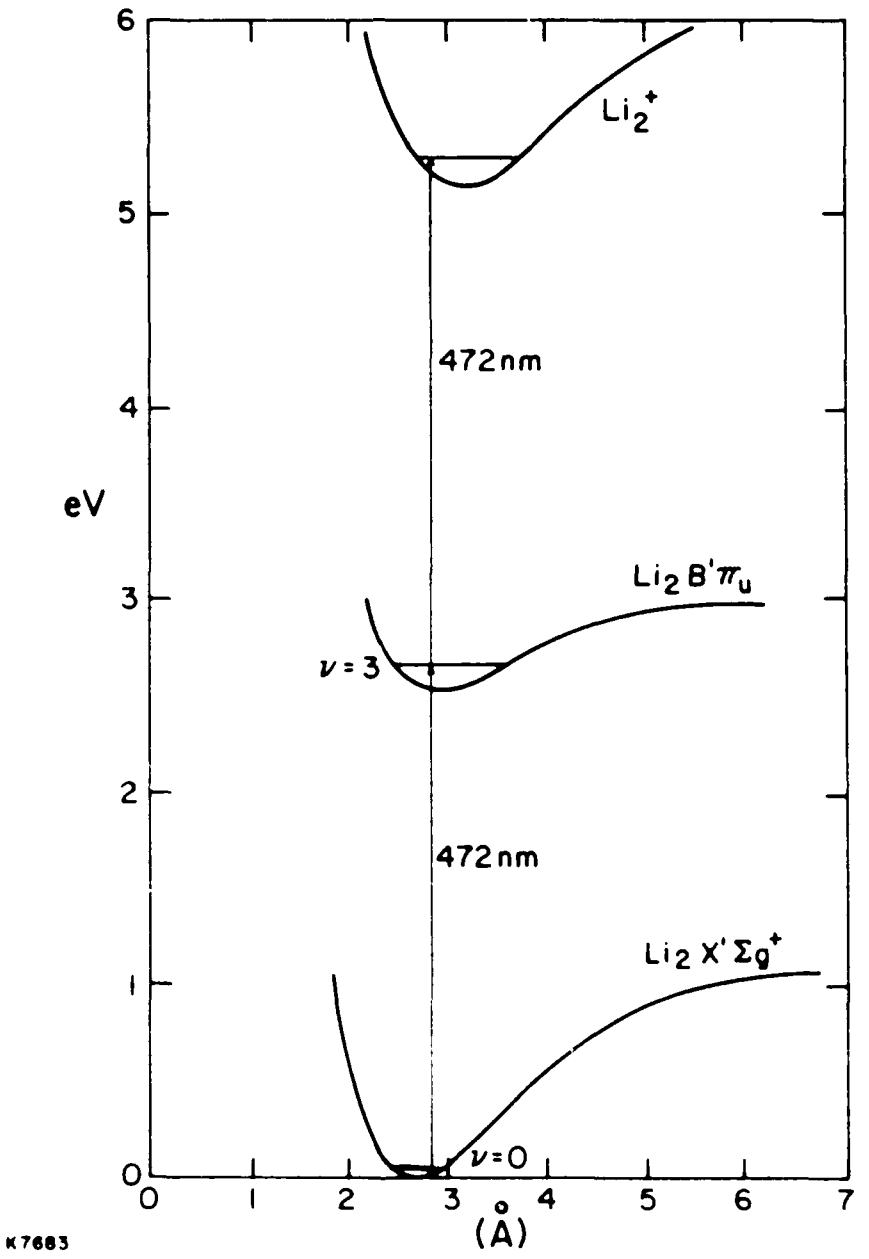

Figure 19 Two-Step Photoionization of Li_2

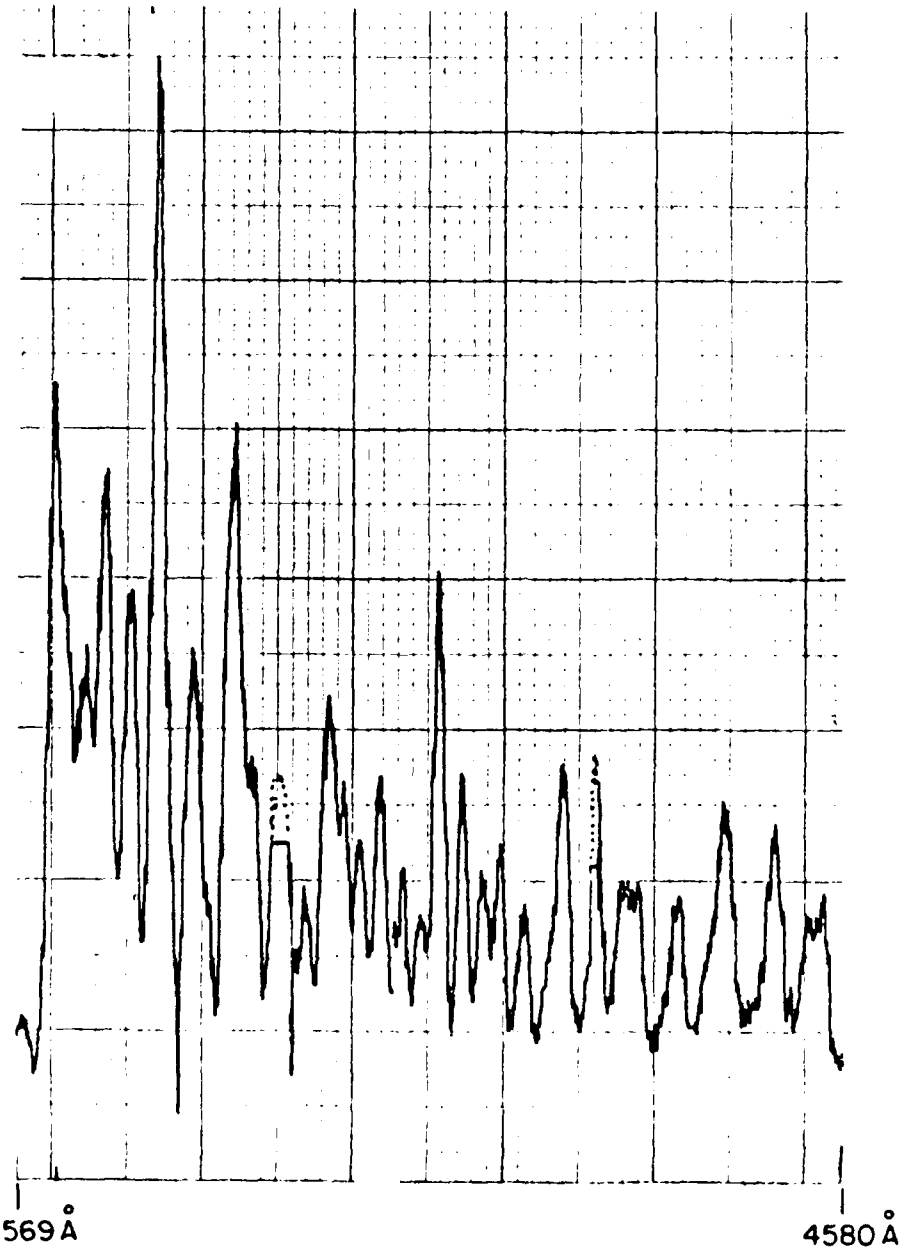

Figure 20 Li_2^* Signal for Excitation via the X - B, 0-6 Band

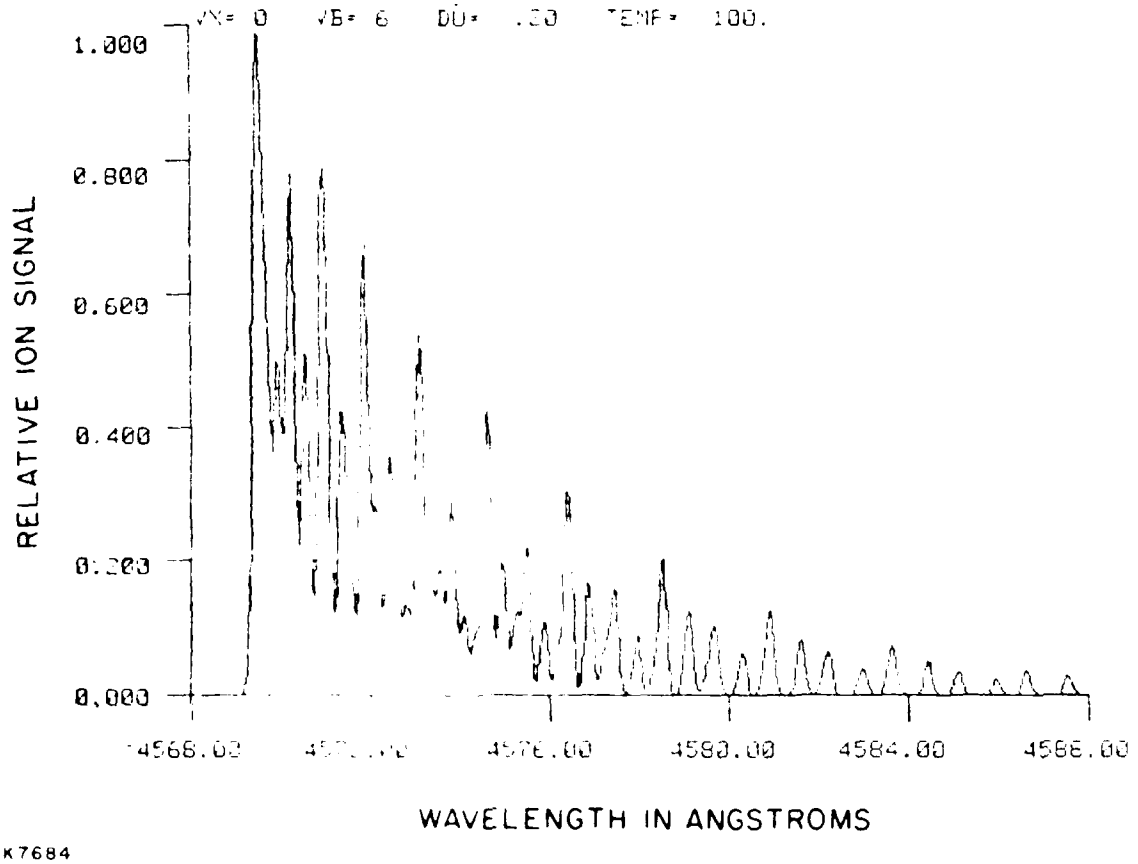

Figure 21 Li_2 C-b Band Computed for 100°K

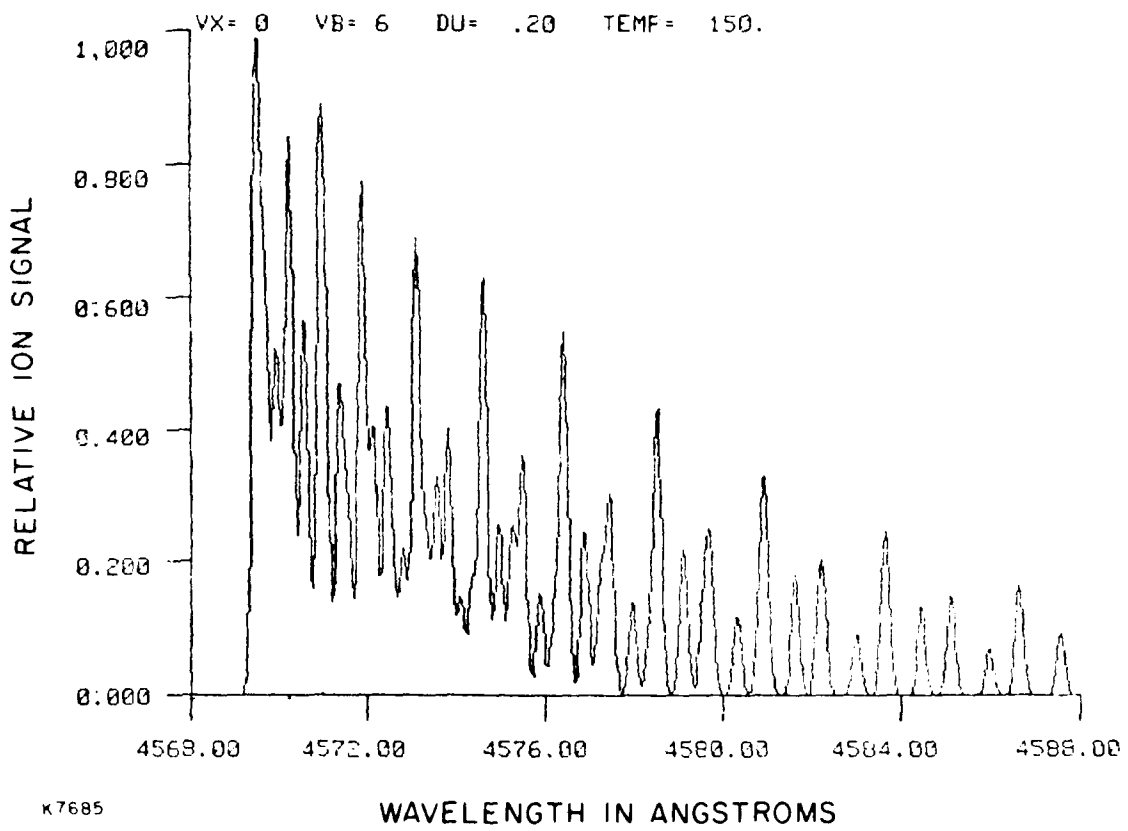

Figure 22 Li_2 0-6 Band Computed for 150°K

using the appropriate [illegible] absolute wavelengths were computed using the spectroscopic constants of Hessel and Vidal.[8] The calculation was performed with a [illegible] Å in order to simulate the limiting experimental resolution.

From the comparison the rotational temperature may be seen to be between 100°K and 150°K. The shape of the spectrum is reasonably well modeled, apart from the height of a peak at 4571 Å, which appears at be ≈ 1.5 times greater than the model would predict. The explanation for this is not obvious. The most likely possibility is that the tunable dye laser went through a longitudinal mode resonance at this point, thus affecting the laser spectral intensity (although not observably varying the laser pulse energy). It is also possible that sharp structures exist in the Li_2 photoionization cross section.

How does this rotational temperature of ≈ 150°K compare with the prediction for this beam? In Section 3.1 above Eq. (3-6) may be used, together with the freezing radius Mach number M = 3.9 which applied for a Li oven temperature of 760°C, to predict a 'freezing temperature' of 170°K. This applies at the artificial point where the beam is supposed to become collisionless, although in reality a gradual transition occurs to collision-free conditions. Nevertheless it is encouraging that the empirical modeling of beam divergence implies a temperature reasonably close to that observed. In going from 760°C to the 800°C at which the 0-6 band was analyzed, a further small decrease in temperature is expected, because the Mach number at the freezing radius increases.

From this measurement and comparison, the rotational temperature is implied to be close in magnitude to the translational temperature, which is to be expected, given that the cross sections for Li-Li_2 rotational relaxation (2×10^{-14} cm^2) is very much greater than that for Li-Li collisions ($\approx 5 \times 10^{-16}$ cm^2). Each Li atom is colliding as frequently with Li_2

7. 'Spectra of Diatomic Molecules,' Herzberg, G., Second Edition p. 208, Van Nostrand, NY.

8. 'The $B'\pi_u - X'\,^1\Sigma_g^+$ Band System of the $^7Li_2$ Molecule,,' Hessel, M.M. and Vidal, C.R., J. Chem. Phys. 70, 4439 (1979).

molecules as it is with other Li atoms. It is therefore to be expected that the 'freeze' in rotational temperature only occurs because of a freeze in translational temperature.

The effectiveness of optical pumping in Li_2 depends upon the fraction of the Li_2 ($v = 0$) population accessed by the pump light. Clearly for the band shapes presented above, high fractional pumping out of the $v = 0$ state requires a broad-band optical pump, of width 10 Å. In the following sections experiments are described in which both narrow-band and broad-band pumping are used.

3.5 SINGLE LINE OPTICAL PUMPING OF Li_2

As one method of creating a population of highly excited Li_2 (X) v^* states in the beam we have employed a dye laser of bandwidth equal to the width of the resolved rotational structure of Figure 20, i.e., 0.25 Å. This laser, when tuned to the B - X band of interest, extracts the population out of a group of rotational levels in the X, $v = 0$ state. The maximum population is accessed when the laser is tuned to the highest peak in a band structure such as that of Figure 20. Taking the 0-6 band as an example we note that the pronounced peak at the band head is composed of the following transitions within a 0.25 Å range (double prime denotes the lower level):

$(v', J'; v'', J'')$	λ (nm)
(6, 3; 0, 2)	456.945
(6, 4; 0, 3)	456.946
(6, 2; 0, 1)	456.951
(6, 5; 0, 4)	456.954
(6, 1; 0, 0)	456.964
(6, 6; 0, 5)	456.969

To pump on the band head with a bandwidth of 0.25 Å therefore accesses the ground state rotational levels $J'' = 0 \rightarrow 5$. By taking the ratio of the area of this peak to the whole band we find that only 8 percent of the Li_2 population is accessed by narrow-band pumping at this beam temperature,

Of the molecules pumped into the B state ~ 50 percent end up in a close group of high vibrational levels in the X state. The molecular radiative decay time is 9 nsec, while the pump laser pulse duration is 5 nsec. During the

pump pulse the group of transitions lying within the pump bandwidth is saturated, with equilibrium populations in the ratio of the degeneracies of the upper and lower levels.

It

$$N_L = \sum_{J''} n_{J''} \tag{3-27}$$

is the lower level population during pumping, the upper level population of the pumped transitions becomes

$$N_u = \sum_{J'} n_{J'} = \sum_{J''} n_{J''} \frac{g_{J'}}{g_{J''}} \tag{3-28}$$

The rate of spontaneous decay of B state molecules is

$$R_S = N_u A_S \tag{3-29}$$

where A_S is the spontaneous emission rate constant (1.1×10^8 sec^{-1}). As a rough approximation $N_u = N_L \doteq 0.5\ N_0$ where N_0 is the initial molecular population accessed by the pump light. This population then is depleted by spontaneous emission according to

$$\dot{N}_0 = -0.5\ N_0 A_S$$

$$\text{or } N_0(t) = N_0 e^{-0.5\ A_S t} \tag{3-30}$$

For a sufficiently long pump pulse all of the accessed population of molecules would undergo spontaneous emission into X (v") states. However, for

finite pulses, because the upper and lower populations have been equal during the pump pulse and the remaining upper population also decays spontaneously after the end of the pulse (duration t_p), the total fraction of the accessed population removed is

$$(1 - 0.5\, e^{-0.5\, A_s t_p})$$

For a nominal 5 μsec pump pulse 62 percent of the accessed population is removed. Of this fraction ~ 50 percent decays into the close X (v") group of states of interest for dissociative attachment. The fraction of accessed molecules pumped usefully is therefore 31 percent.

We have performed an experiment to monitor the removal by optical pumping of the group of rotational levels in Li_2 (v = 0) which contribute to the 0-4 bandhead peak. In this experiment optical pumping was performed by a single 0.25 Å pulse at 4669.2 Å. After a delay of 100 nsec a more intense probe pulses was scanned through the 0-4 band to generate a Li_2^+ signal. The data is shown in Figure 23 where the presence of the pump may be seen to cause a 47 percent reduction in bandhead intensity (after adjustment for signal magnitude). Because of the difficulty of alignment in this measurement, this observation was subject to an underestimation error and the real reduction could have been greater than this. As the calculation above shows, a 62 percent reduction in population was expected theoretically. Incidentally this measurement implies that the frequency of rotational collisions in the beam is $<< 10^7\ sec^{-1}$.

Combining the above 8 percent and 31 percent ratios we estimate that 2.5 percent of all Li_2 (v = 0) molecules are pumped into high vibrational levels in our experimental conditions for narrow-band optical pumping.

At a Li oven temperature of 800°C the beam density is $1.6 \times 10^{13}\ cm^{-3}$ in the experimental region of which 4 percent are Li_2 molecules. Pumping 2.5 percent of these gives $1.6 \times 10^{10}\ cm^{-3}$ Li_2 (X, v") molecules available for dissociative attachment.

Because the beam is essentially collision free at this point (Section 3.1) these excited molecules are metastable over times > 10^{-5} sec.

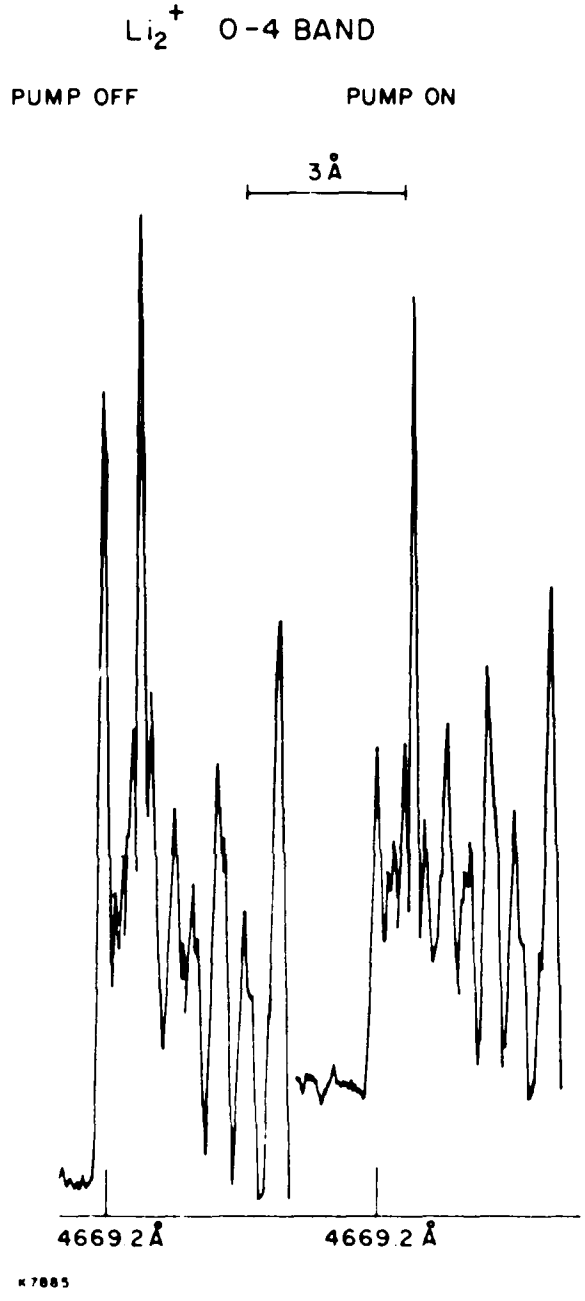

Figure 23 Reduction of 0-4 Bandhead Line Due to Narrowband Optical Pumping. Monitored by Li_2^+ signal.

3.6 BROAD BAND OPTICAL PUMPING OF Li_2

We have performed experiments in which a broad band (10 Å) dye laser was used to simultaneously pump all the rotational transitions in a vibrational band of Li_2. The laser we employed was a flashlamp-pumped dye laser of 1.5 μsec pulse duration and maximum blue output energy of ≈ 2 mJ in the 10 Å bandwidth. It could be pulsed at up to 4 Hz, but suffered from poor pulse-to-pulse reproducibility and an output which decayed (for either thermal or chemical reasons) with a 1/e time of 3 min. After a 10 min wait, the output would fully recover. This behavior could be attributed to the fact that the laser concerned was a laboratory prototype, based on 1975 technology, which had not been engineered for long-term operation. Nevertheless, a high degree of optical pumping was observed during the first 2 min of dye laser operation. This work will be discussed in its present state although an improved flashlamp-pumped dye laser recently purchased by AERL will be used for further work.

An estimate may be made of the degree of pumping to be expected in this experiment. For an isotopic molecular gas the absorption cross section is

$$\sigma(\nu) = \frac{3\lambda_{jk}^2 \left|\langle \nu' \mid \nu'' \rangle\right|^2 g\,(\nu - \nu_{jk})}{8\pi t_{rad}} \qquad (3\text{-}31)$$

where

λ_{jk} = the transition wavelength

$\left|\langle \nu' \mid \nu'' \rangle\right|^2$ = Franck-Condon overlap factor for the transition ($\nu''J'' \rightarrow \nu'J'$)

t_{rad} = radiative lifetime of the upper level

$g(\nu - \nu_{jk})$ = normalized line shape function, i.e.,

$$\int_0^\infty g\,(\nu - \nu_{jk})\, d\nu = 1$$

For the (v'', v') = (0, 5) transition (at 461.8 nm) the overlap factor is 0.0126.[8] Since t_{rad} = 8.5 nsec,[9] we obtain for a Doppler-broadened line at 150°K, $\sigma(\nu_{jk}) = 1.24 \times 10^{-13}$ cm^2. The saturation energy for optical pumping $h\nu/\sigma$ is therefore 3.4 μJ cm^2.

For optical pumping on this transition to reach 1/e saturation after 1.5 μsec, a laser intensity of 2.27 W/cm^{-2} is required within the 3 GHz Doppler linewidth. In a 10 Å bandwidth this equals 1.06 kW/cm^2.

For the present experiment, in which 2 mJ were delivered in 1.5 μsec to 1 cm^2 of the Li beam the laser intensity was 1.3 kW/cm^2, sufficient to just saturate the transition according to the above estimate (molecules reaching the B state decay into a X (v'') distribution determined by the Franck-Condon factors).

Experimentally the depletion of the Li_2 (v = 0) level was monitored by the Li_2^+ signal from a N_2-pumped dye laser (10 μJ, 5 nsec) tuned to the 0-3 transition. This probe, or monitor, laser was fixed 1 μsec after the end of the 1.5 μsec flashlamp dye laser pulse. The data collection was complicated by the fact that the broad-band optical pump laser also created a Li_2^+ signal of about the same size as that from the monitor laser. The ideal experimental effect, for a constant optical pumping laser energy, is shown in Figure 24a. In practice the pumping laser was decaying with time, leading to an effect like that in Figure 24b. Actual data traces are shown in Figure 25. This data is of a preliminary nature and is marred by the electrical interference of the flashlamp-pumped laser as well as its erratic pulse-to-pulse behavior. There is evidence of a v = 0 depopulation of up to 40 percent in some of the traces we have obtained. Improved data should become available with the new dye laser which is being installed.

Preliminary work with broad-band optical pumping has therefore demonstrated the removal of up to 40 percent of the X (v = 0) population. Of those molecules pumped, 50 percent decayed into a group of levels close to v = 10 in the Li_2 (X) manifold. Given the initial Li_2 density of 6 x 10^{11} cm^{-3}, we therefore infer an excited vibrational population density of 1.2 x 10^{11} cm^{-3} in a group of levels of interest for dissociative attachement.

9. 'Radiative Lifetimes of the $B^1\pi_u$ States of Li_2,' Uzer, T., Watson, D.K. and Dalgarno, A., Chem. Phys. Lett. 55, (1978).

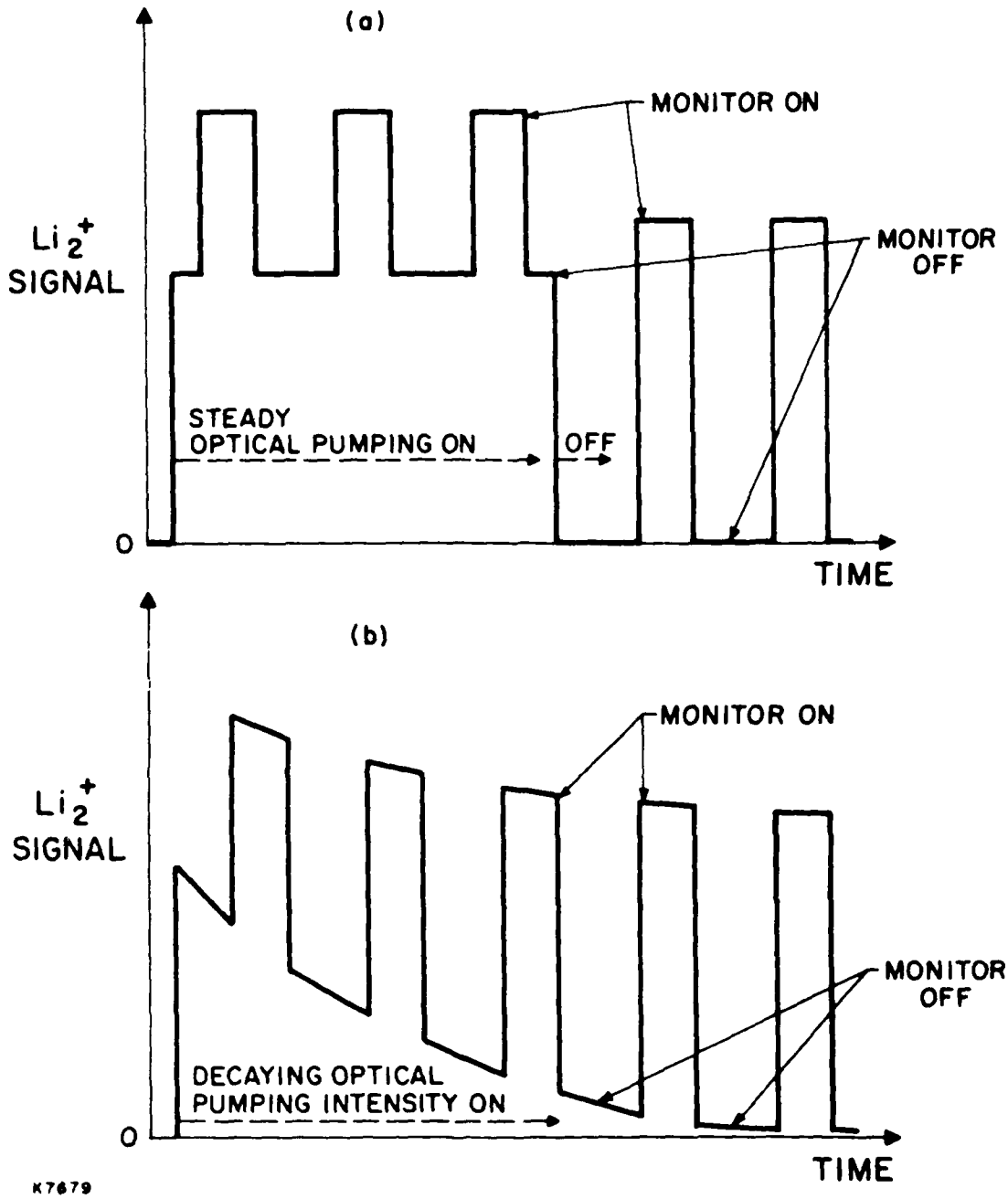

Figure 24 (a) Reduction in Monitor Li_2^+ Signal Due to Steady Optical Pumping; (b) Reduction in Monitor Li_2^+ Signal Due to Optical Pumping at Decreasing Intensity

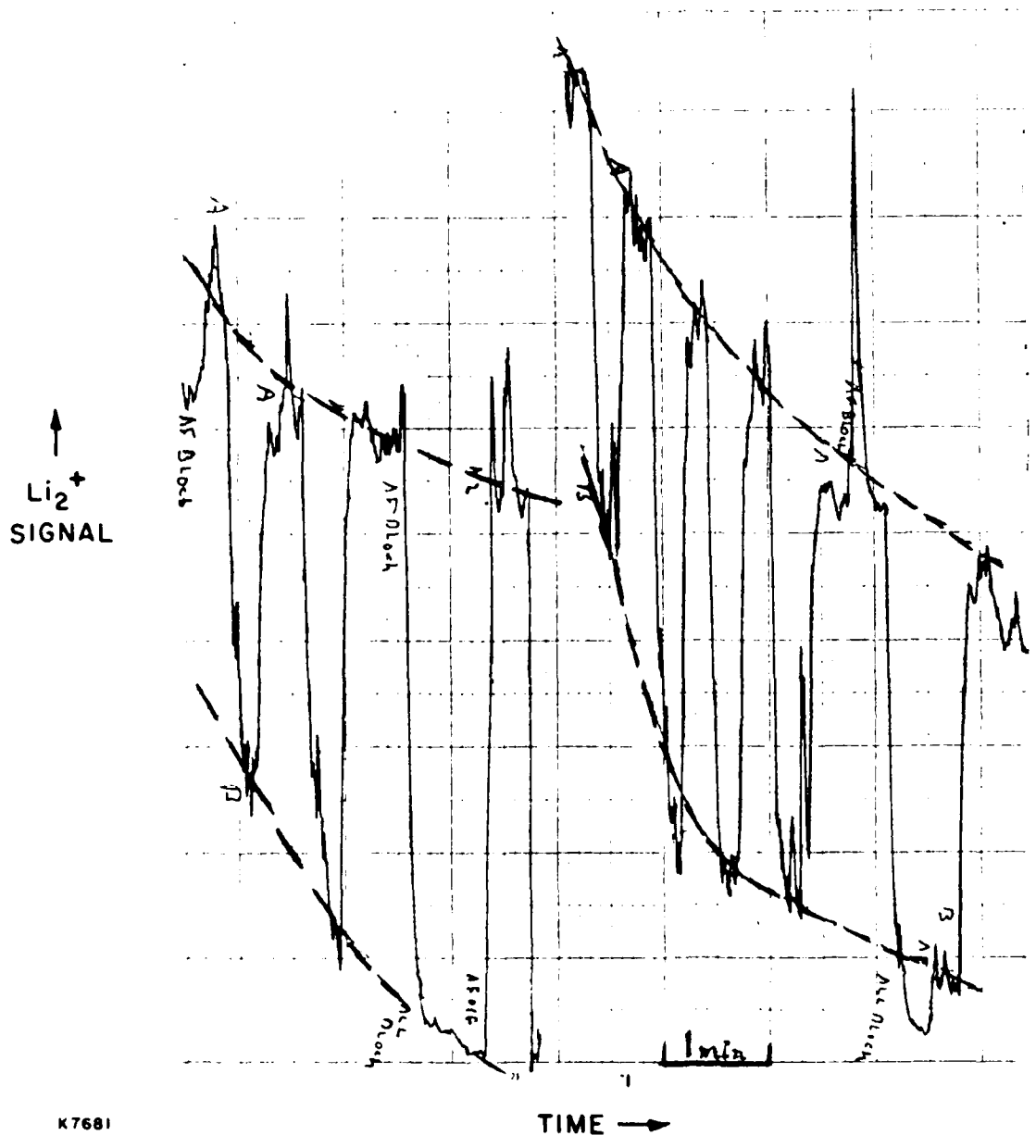

Figure 25 Measured Broad-Band Optical Pumping: Pump 0-6, Monitor 0-3

3.7 MEASUREMENTS OF DISSOCIATIVE ATTACHMENT

To date we have only partially explored the range of conditions available in this experiment, and have consequently only been able to place an upper bound on the dissociative attachment rate constant for groups of Li_2 (X) levels centered on $v^* = 9.5$ and $v^* = 11$.

In the experiments we measured the Li^+ signal due to the photoionization of Li (Section 3.2), and then reversed the extraction polarity to look for Li^- ions, with or without optical pumping of Li_2. The experiments are best discussed under the separate headings of narrow- and wide-band optical pumping.

(a) Narrow-Band Optical Pumping

When two N_2-pumped dye lasers are used for photoionization and a third is used for optical pumping the experiment may be run at 60 Hz with a Li^+ signal-to-noise ratio of 1.0×10^4. This implies that we are able to detect the attachment of one electron in 10^4 to form a Li^- ion. We have observed complete suppression of the electron signal at this level by the crossed magnetic field section of the drift tube and we are assuming that the collection efficiency for Li^- is no different from that for Li^+. Although the extraction pulse was applied 2 μsec after the electrons were created, the plasma expansion did not allow interaction of e^- with Li_2 (v^*) for more than a fraction of 1 μsec. Precisely how long depended on the electron energy relative to the threshold energy for dissociative attachment, as discussed in Section 3.3, (Eq. (3-26)). For the present photoelectron energy of 0.53 eV, and a threshold $\epsilon_{DA} = 0.25$ eV (for example), the interaction time is $t_{DA} = 0.34$ μsec.

For a $Li^-:Li^+$ signal ratio $\leq 10^{-4}$ we require

$$n \left\{ Li_2 (v^*) \right\} k_{DA} t_{DA} \leq 10^{-4}$$

Using n from Section 3.5 ($n = 1.6 \times 10^{10}$ cm^{-3}) we obtain $k_{DA} \leq 1.8 \times 10^{-8}$ cm^3/sec^{-1}. This is the experimental upper bound obtained from $v^* = 9.5$ in the case of single-line optical pumping. It contains an assumption about the threshold energy for dissociative attachment from these states.

(b) Broad-Band Optical Pumping

The broad-band laser pumped Li_2 more effectively (Section 3.6), but suffered from the experimental disadvantages of;

1. Output decaying to zero over 5 min,
2. ± 50 percent fluctuations in pulse-to-pulse energy,
3. Severe electrical interference from the flashlamp drive current pulse,
4. A repetition rate of 4 Hz, giving poor signal-averaging.

Using this laser the experimental resolution was ~ 10 times worse than that of the narrow band case, i.e., in $Li^-:Li^+$ ratio of 1×10^{-3} was the lower limit of detection.

As discussed in Section 3.6 the 0-6 transition was pumped to give 1.2×10^{11} cm^{-3} Li_2 ($v^* = 11$) states. Using the same t_{DA} assumption as above,

$$n \left\{ Li_2 (v^*) \right\} k_{DA} t_{DA} \leq 10^{-3}$$

gives $k_{DA} \leq 2.4 \times 10^{-8}$ cm^3/sec^{-1}. Again, it should be emphasized that this rate constant contains an assumption about the threshold energy for dissociative attachment from $v^* \approx 11$ states, i.e., $\varepsilon_{DA} = 0.25$ eV.

In the following section the potential for increased experimental resolution is explored.

4.0 FUTURE EXPERIMENTS

4.1 SCOPE FOR INCREASED SENSITIVITY IN DISSOCIATIVE ATTACHMENT MEASUREMENT

There are four ways by which the experimental resolution of k_{DA} can be improved beyond that reported in the previous section:

i. Use of a larger number of electrons and Li^+ ions.

ii. Increase of Li_2 (v^*) density through the use of higher beam density and improved broad-band optical pumping.

iii. Increase of the interaction time t_{DA} by using a larger diameter of plasma column.

iv. Use of an electron multiplier in place of the ion collector plate.

It is proposed to perform an experiment in which both the ionization and the optical pumping are performed by a single 1 μsec pulse blue laser. This process is illustrated schematically in Figure 19 for pumping via the $v = 3$ level in the B state, but we would pump higher levels up to a limit of $v \approx 9$, as discussed below (and illustrated in Figure 1). The laser in question can deliver 100 mJ in a 10 Å band with a ~ 1 μsec pulse duration. It has a repetition frequency of 10 Hz, which should allow good signal-averaging.

An analysis may be made of the ionization efficiency for two-step photoionization. Let I be the pump laser intensity and $\Delta\nu_L$ its frequency bandwidth. The rate constant for removal of Li_2 (X) ($v = 0$) states by optical pumping is

$$k_{PUMP} = \frac{3}{8\pi} \frac{\lambda^2 F I}{h\nu\, t_{RAD}\, \Delta\nu_L} \qquad (4\text{-}1)$$

where λ is the wavelength, $h\nu$ is the photon energy, F is the Franck-Condon factor and t_{RAD} is the Li_2 (B - X) radiative lifetime.

Of the molecules reaching the Li_2 (B) state a fraction decays to Li_2 (X) (v^*) levels and the rest are photo-ionized to $Li_2^+ + e^-$. The rate constant for photoionization is

$$R_{PI} = \frac{I\ \sigma_{PI}}{h\nu} \tag{4-2}$$

The fraction of pumped molecules which is photoionized is

$$\theta = \frac{R_{PI}}{R_{PI} + \frac{1}{t_{RAD}}} \tag{4-3}$$

Given experimental conditions in which we assume that the 100 mJ, 1 μsec pulse is spread over a 1 cm^2 cross section, $I = 10^5$ W/cm^2. For complete optical pumping in 1 μsec we require $R \geq 10^6$ sec^{-1} and hence, by Eq. (4-1)

$$F \geq 2.3 \times 10^{-4} \tag{4-4}$$

This implies that we may only pump up as far as the 0-9 transition (444 nm) for which $F = 1.3 \times 10^{-4}$.

Assuming that Eq. (4-4) is satisified, the fraction of Li_2 (X) molecules ionized is given by Eq. (4-3). Assuming $\sigma_{PI} = 3 \times 10^{-17}$ cm^2 we obtain $\theta = 0.054$.

Using the above numbers we may estimate the experimental sensitivity for k_{DA}.

Let us suppose that the beam density is given by the maximum achievable in this apparatus $n(Li) = 8 \times 10^{13}$ cm^{-3}, with 5 percent dimer, i.e., $n(Li_2) = 4 \times 10^{12}$ cm^{-3}. For complete optical pumping, as described above, $n\{Li\ (X)\ (v^*)\} \doteq 4 \times 10^{12}$ cm^{-3}. The Li_2^+, e^- plasma density is $\theta \times n(Li_2) = 2.2 \times 10^{11}$ cm^{-3}.

Because the plasma column diameter is larger, its expansion occurs more slowly and t_{DA}, the interaction time for electrons, is greater than in the previous work (Section 3.7). If the 1 cm^2 beam is of circular section its radius r_{eo} = 0.56 cm. For photoionization at 444 nm the photoelectron energy ε_o = 0.45 eV. Using Eq. (3-21),

$$\gamma = \frac{1}{r_{eo}} \sqrt{\frac{2\varepsilon_o}{m_i}} = 4.4 \times 10^5 \text{ sec}^{-1} \tag{4-5}$$

and from Eq. (3-26)

$$t_{DA} = - 2.27 \times 10^{-6} \cdot n \left[1 - \sqrt{1 - \frac{\varepsilon_{DA}}{\varepsilon_o}} \right] \tag{4-5}$$

where ε_{DA} is the threshold energy for dissociative attachment.

If we assume that the ion detection limit is at the same noise level as in the previous experiments (Section 3.7), the increased number of electrons in this experiment should allow the measurement of 1 x 10^{-6} attachment probability. The sensitivity on k_{DA} is therefore

$$k_{DA} < 10^{-6}/n\,(Li_2^*)\, t_{DA}$$

$$\text{or } k_{DA} < - 1.1 \times 10^{-13}/n \left[1 - \sqrt{1 - \frac{\varepsilon_{DA}}{\varepsilon_o}} \right] \tag{4-6}$$

This function is plotted in Figure 26 for the case of ε_o = 0.45 eV corresponding to 0-9 pumping.

Reviewing the above we conclude that an experimental determination of k_{DA} with very good resolution should be possible using two-step photoionization and broad-band pumping, both performed by the same blue laser.

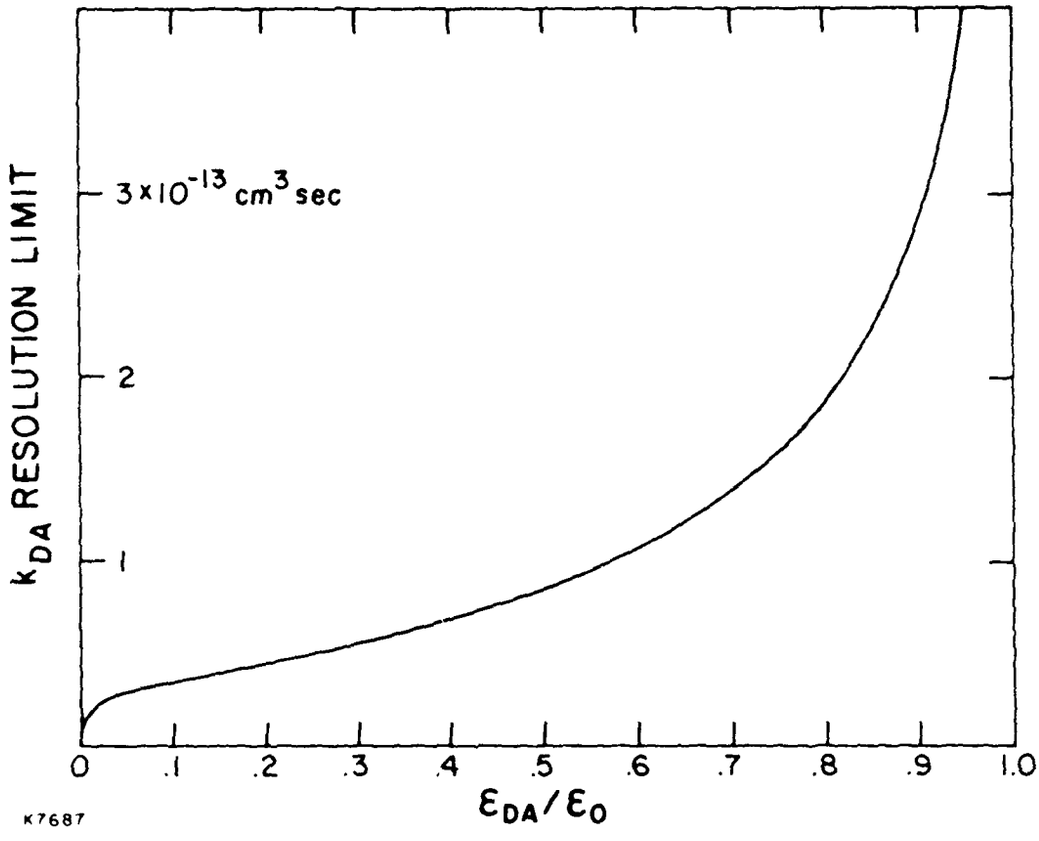

Figure 26 Resolution Limit for Dissociative Attachment as a Function of Threshold

Other combinations of laser are possible; but do not give such good resolution. For instance, to create the $Li^+ + e^-$ plasma by three-step photoionization of Li and to perform optical pumping with the 100 mJ blue laser would give a resolution of $k_{DA} \leq 1 \times 10^{-10}$ cm^3/sec^{-1}. Nevertheless this technique would have to be used if k_{DA} were to be studied as a function of ϵ_o, the electron energy.

The use of an electron multiplier would make an estimate of the $Li^-:Li^+$ current ratio much less direct and would decrease the accuracy of any k_{DA} determination.

4.2 PHOTOIONIZATION OF Li_2 (B) STATE

The present experiment, operating at moderate temperatures ($\simeq 800^\circ C$) and using the 10 mJ, 60 Hz N_2-pumped dye lasers, is capable of yielding good signal-to-noise data of Li_2^+ formed by the photoionization of Li_2 (B). This process is illustrated for the $v' = 3$ level in Figure 19, and a typical spectrum is shown in Figure 20. A further measurement which is of considerable scientific interest may be obtained in the same conditions, namely the wavelength dependence of the photoionization cross section of the Li_2 (B) state. To obtain this two blue lasers are used, one at a fixed frequency to select a given Li_2 (B) (v', J') state and the second one to scan in wavelength from the photoionization threshold onwards.

The accumulation of this new data for Li_2, in ultracold beam conditions, would provide a very useful benchmark for testing theoretical models of molecular photoionization and for the evaluation of the ab initio methods in quantum chemistry.

END

DATE
FILMED

9 — 83

DTIC